SOME CLIMATOLOGICAL AND ENERGY BUDGET CALCULATIONS USING THE FGGE III-b ANALYSES DURING JANUARY 1979

Masao Kanamitsu*

ECMWF

* on leave from Electronic Computation Centre,
Japan Meteorological Agency

ABSTRACT

The analyses of complete data sets (level II-b) of the First GARP Global Experiment during January 1979 at the European Centre for Medium Range Weather Forecasts are examined from climatological and diagnostic points of view. Comparison with long time averaged climatology is performed. Some differences are discussed in relation to the data coverage.

The tropical velocity potential field for the monthly mean wind is presented. Effects of the initial guess and the initialization are discussed.

The kinetic energy budget in zonal wavenumber domain is computed, and results are compared with other studies. Interesting differences of energetics between the hemispheres are found. It is shown that the energetics of the ultralong wave has large latitudinal and temporal variations in the northern hemisphere.

1. INTRODUCTION

The main objective of 4-dimensional assimilation is to provide the best initial state for the numerical prediction of the atmospheric flow. Accordingly, the analysis must depend in some degree on the particular prediction model. This dependency is usually established by the use of the forecast fields obtained from the prediction model. The quality of the analyses is evaluated through the final product of the numerical prediction.

Four-dimensional data assimilation has been used at the European Centre for Medium Range Weather Forecasts (ECMWF) for the analysis during the First GARP Global Experiment (FGGE), Lorenc (1980). The products will be used not only for prediction experiments but also for many other research purposes. The analysis have been extensively tested from the prediction point of view and reported elsewhere (e.g. Bengtsson and Källberg, 1980). To use the analyses for other research purposes, namely for various diagnostic studies, it is essential that the analysed variables are physically consistent. In this sense, an analysis scheme with some dynamical constraint and properly balanced initial guess fields becomes important, while excessive dependency of the analysis on the particular prediction model is not favourable.

The purpose of this study is to examine the validity of the use of analysis for budget studies. Two kinds of studies can be noted here, namely the long time average characteristics of the analyses and special event case studies.

In this paper, we have performed monthly averaged budget calculations. We concentrate on the January mean but similar calculations are in progress for other months, and will be reported later.

2. ANALYSIS OF THE FGGE DATA

The analysis scheme used is documented in detail by Lorenc (1980). Several special observations are incorporated by assigning proper observational errors (Bengtsson and Källberg, 1980). Major differences with conventional (non-FGGE) observation networks are the enhanced cloud winds from four satellites covering nearly the entire globe (50^{o}S - 50^{o}N) providing mostly low (~850 mb) and high (~200 mb) winds, southern hemisphere drifting buoys, satellite soundings and several types of special tropical observations. The major improvement in analyses is expected over the tropics and over the southern hemisphere.

At the ECMWF, several different types of archived analyses are available (uninitialized/initialized; spectral coefficient/grid point; p-surface/σ-surface; packed/unpacked). In this study, packed grid point uninitialized pressure-surface fields are used. This type of field is compact enough to handle long sequences of analyses and fit of the analysis to the observations is best. Other types of files go through modifications by one or combined procedures of p to σ interpolation, initialization, σ to p interpolation and spectral truncation, and can be significantly different from original analysis. Initialized fields are useful in the sense that the variables are physically balanced. However, since the initialization procedure (nonlinear normal mode initialization) depends strongly on the forecast model and the physics included, the use of initialized fields is avoided. In fact, it is shown later that the initialization has some difficulties in keeping analysed large scale divergence in the tropics.

The analyzed variables are surface pressure (p_s), geopotential height (z), east-west component of the wind (u) and north-south component of the wind (v). Humidity is also analysed but is not examined in this study. The analyses of these variables are available at standard pressure levels (15 levels from 1000mb up to 10mb) on an N48 grid (1.875 latitude/longtitude grid resolution). Analyses have been archived every 12 hours (6 hours during special observing period), and all the averages computed in this study are from 12 hour interval analyses. It is noted that all other variables that appear in this paper (e.g. temperature, divergence, omega, etc.) are computed from analyzed variables (the so called III-b archived FGGE format files include uninitialized z, u, v, p_s and initialized temperature and vertical motion fields).

3. JANUARY MEAN FIELD

To make comparison, the normal January climatology used at ECMWF (obtained from NCAR) for northern and southern hemispheres, and the tropical climatology (seasonal mean fields) by Newell et al (1972) are presented together with the January 1979 mean fields. The southern hemisphere normal climatology and tropical mean fields are based on sparse observations such that the difference can be due to the FGGE data coverage as well as to the year to year variations. It is also noted that the tropical climatology is based on time averaged observations and not on average of the analyses.

3.1 Northern hemisphere

3.1.1 Surface pressure (Fig.1)

Several large deviations from normal are noted as follows.

(i) Very weak Icelandic low.

(ii) Intense Aleutian low.

(iii) Intense Siberian high.

(iv) Weak subtropical highs.

These anomalous states over the high latitudes are the results of intense blocking which persisted over Alaska (first half of the month) and over Greenland (last half of the month).

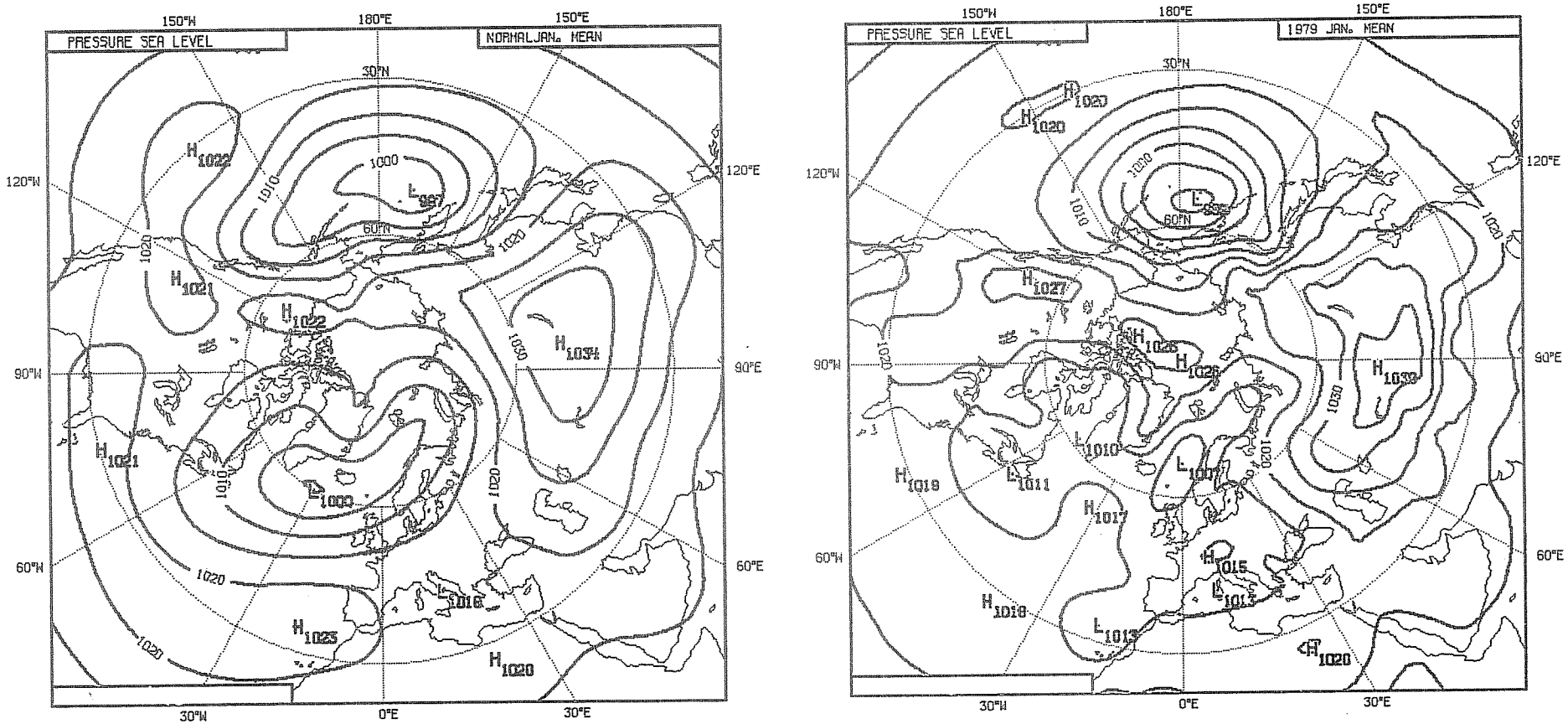

Fig. 1 Northern hemisphere surface pressure pattern. Long time averaged January mean (left) and January 1979 mean from ECMWF analyses (right). Units in mb. Contour interval is 5 mb.

3.1.2 500 mb height (Fig. 2)

As a result of the blockings, ridges over Alaska and northern Atlantic are very intense.

These somewhat anomalous states during January 1979 should be kept in mind when interpreting some of the results shown later.

3.2 Southern hemisphere

3.2.1 Surface pressure (Fig. 3)

Due to the large amount of surface observation by drifting buoys (average 150 buoys), a quite detailed pressure distribution has been obtained. The lows located around 60°S are 3-4 mb lower than the normal climatology compiled from less observations. The subtropical highs are higher by 2-4 mb and as a result, the pressure gradient in the middle latitude zone is larger. The high located off the east coast of South America (40°S, 45°W) has not been depicted in the (normal) climatology.

3.2.2 500 mb geopotential height (Fig. 4)

At this level the main extra data sources are the satellite temperature soundings and the cloud winds. Zonal assymetry is more pronounced than in the (normal) climatology; specifically, the troughs around 40°W and 90°W are very distinct. Dominance of zonal wavenumber 5 is noted, which is also clear in the surface pressure field (Fig. 3).

3.3 Tropics

3.3.1 850 mb wind field

In general, the major large scale features are similar to climatology (Fig. 5). The following differences are noted.

(i) Larger equatorial westerly zone (extending from 60°E to 160°W)

(ii) Distinct trough located off the east coast of South America, separating the south Atlantic subtropical high into two.

(iii) Weaker subtropical highs in the northern hemisphere and the trough at the west coast of Africa. These differences are more likely due to year to year variations.

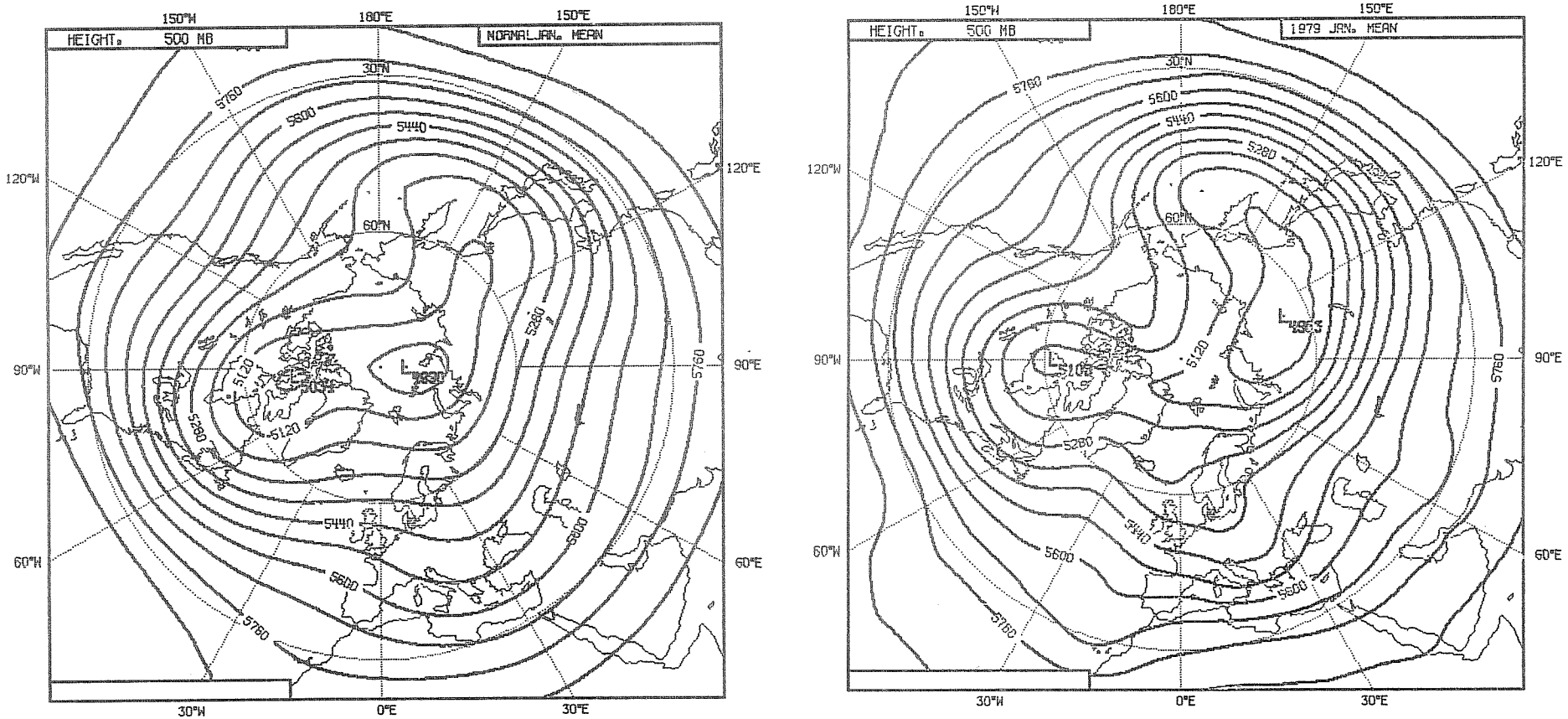

Fig. 2 Same as Fig. 1 but 500 mb height. Units in m. Contour interval is 80 m.

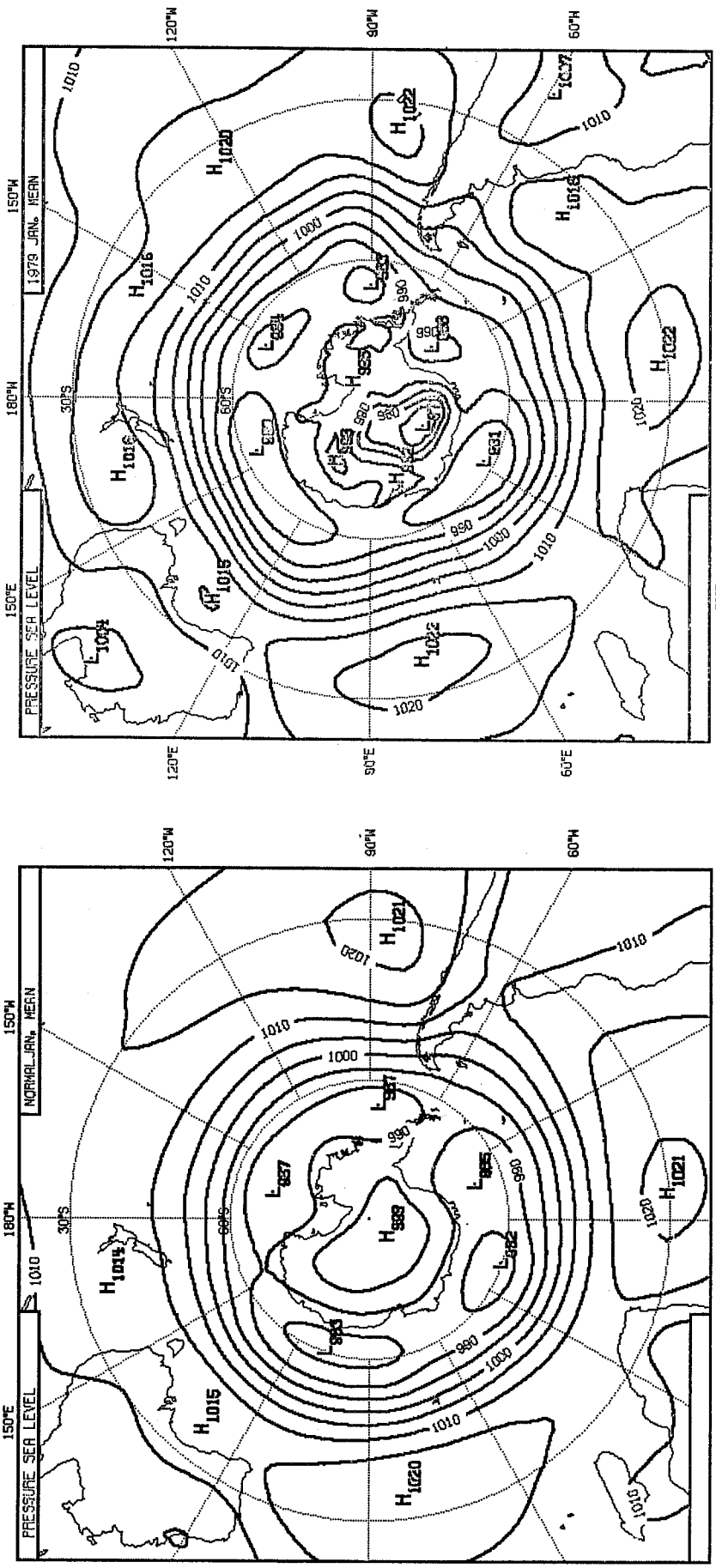

Fig. 3 Same as Fig. 1 but southern hemisphere

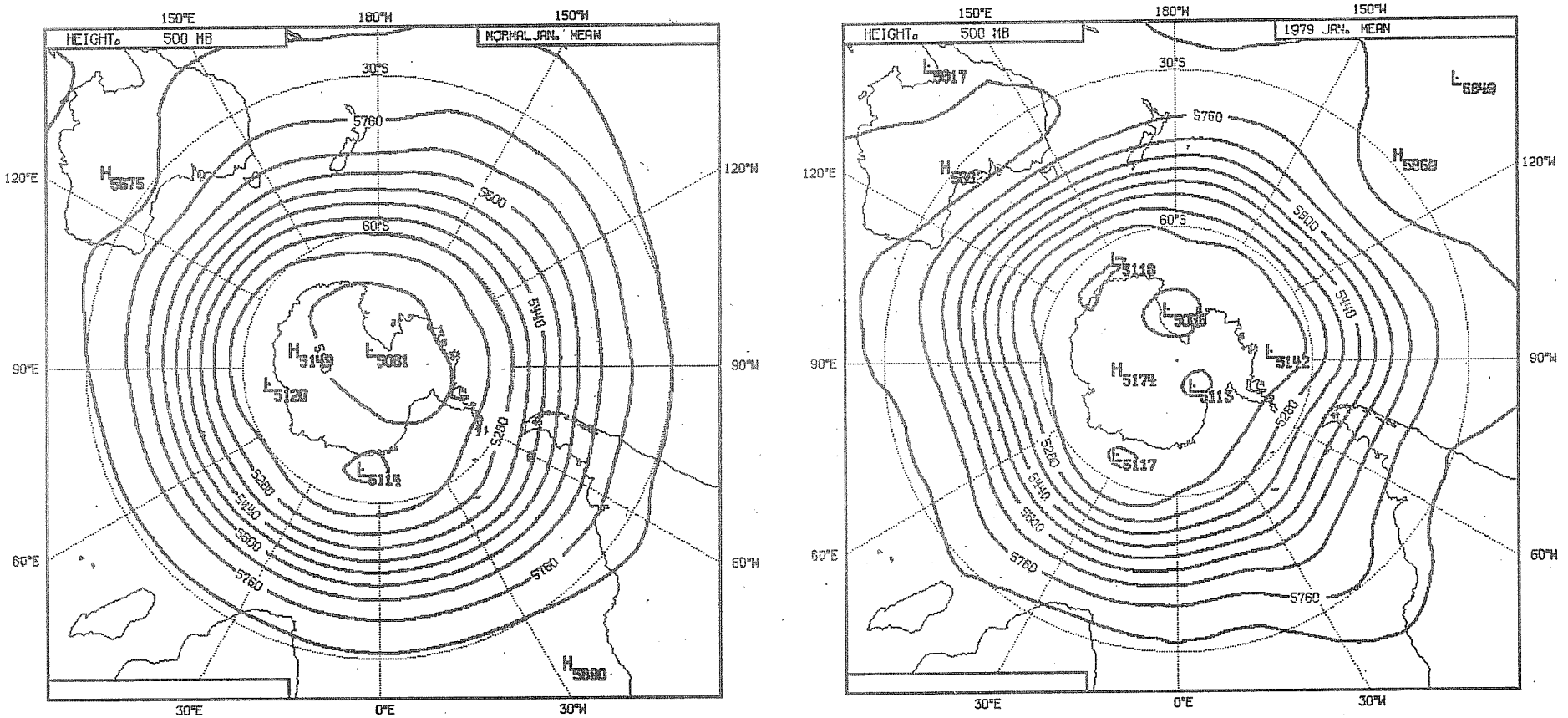

Fig. 4 Same as Fig. 2 but southern hemisphere

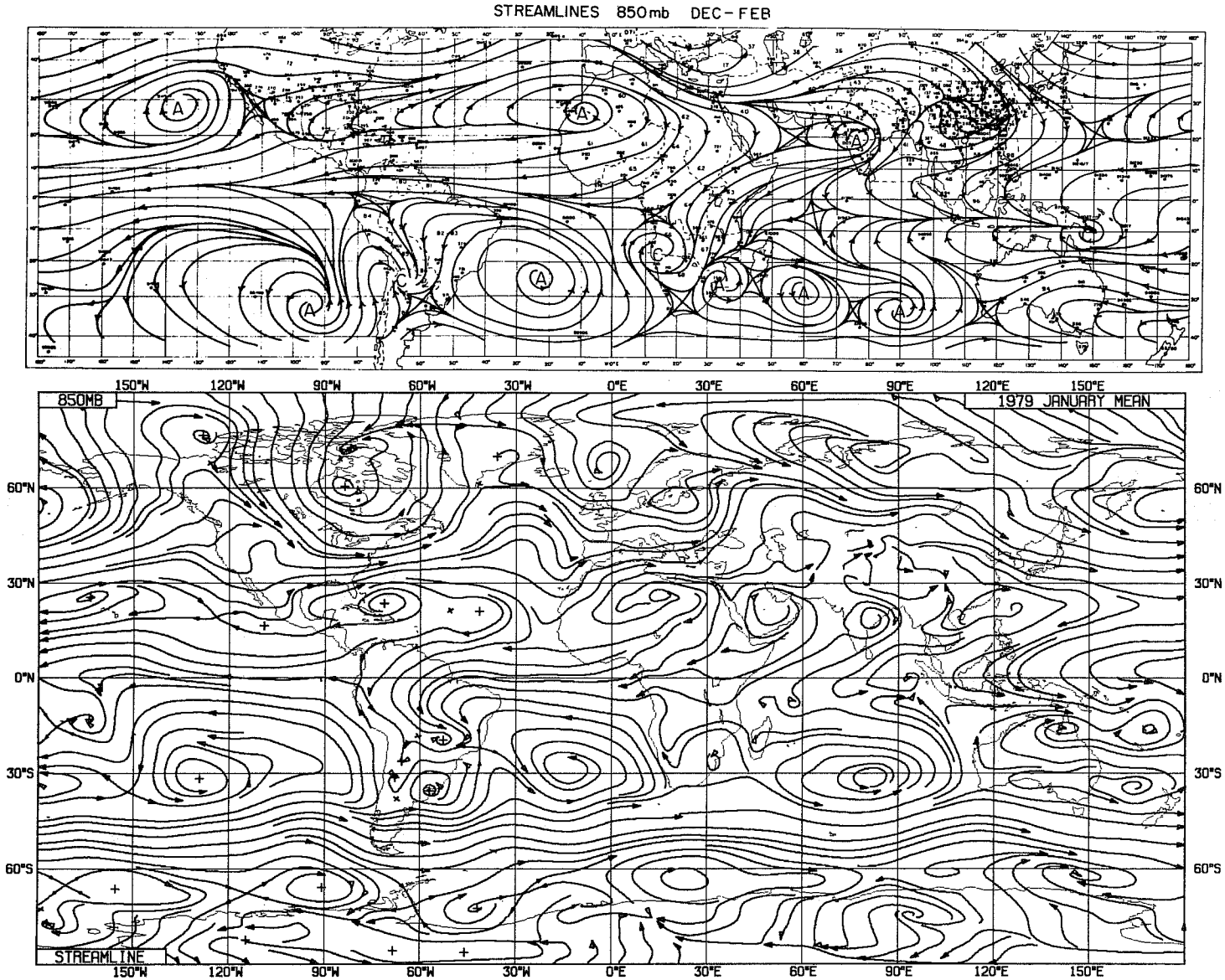

Fig. 5 850 mb streamlines. Winter average in the tropics by Newell et al, 1972 (top). ECMWF January mean (bottom) over the globe.

Zonal winds (Fig. 6) are much larger than in Newell's mean, partly due to the duration of averaging and the data coverage. The differences are largest over the equatorial eastern Pacific and the equatorial Atlantic, where conventional data coverage is very poor.

A strong equatorial westerly jet (~15 m/sec) exists in the area between Australia and New Guinea. The jet is strongest at 850 mb and becomes weaker above and below. This jet is observed only in January and is much weaker in February.

Magnitudes of the meridional wind of the ECMWF analysis (Fig. 7) are also larger than the climatology. The largest differences are observed over ocean areas, particularly over the southern hemisphere and Indian ocean.

Three areas of strong cross equatorial northerlies are noted, over the Amazon basin, the east coast of Africa (in very narrow zone, somewhat resembling the Somali jet in the summer monsoon season but reversed in direction) and Indonesia. The westerly jet over southern New Guinea corresponds to the zone of strong convergence in the meridional wind field.

3.3.2 200 mb wind field

Major flow patterns at this level (Fig. 8) are also very similar to Newell's. Some differences are again observed over the ocean areas.

(i) The trough over Mexico extends to the southern hemisphere (100^{o}W).

(ii) Very sharp trough with strong tilt from north west to south east is located at 140^{o}-120^{o}W, 40^{o}S- equator.

(iii) Weak vortex is located at the equator in the Indian ocean.

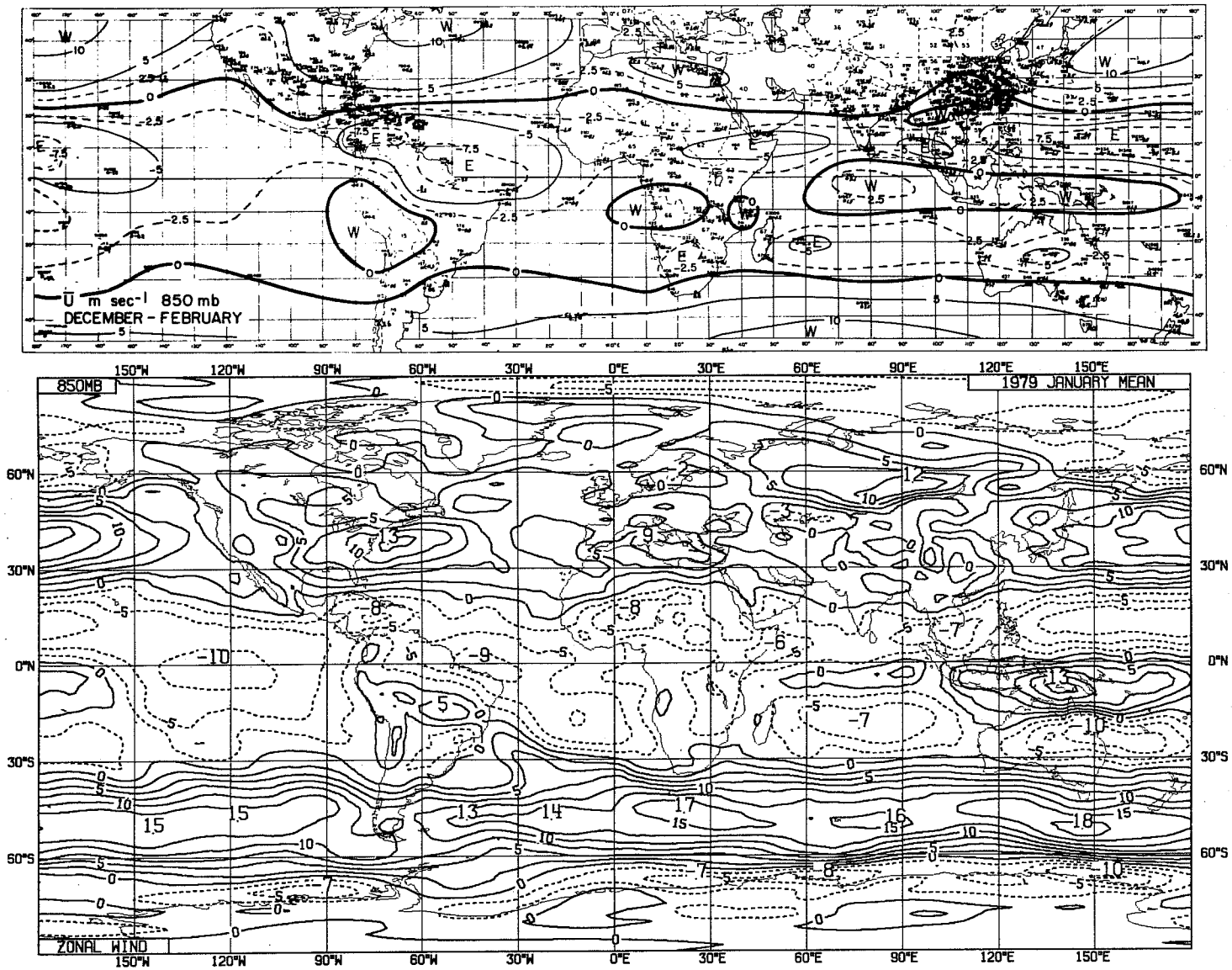

Fig. 6 Same as Fig. 5 but zonal wind, units in m sec^{-1}. Contour interval is 5 m sec^{-1} for Newell's and 2.5 m sec^{-1} for the ECMWF analysis. In the bottom figure, isolines for the negative values are indicated by dashed lines. In the top figure dashed lines indicate intermediate contour levels (2.5 m sec^{-1}).

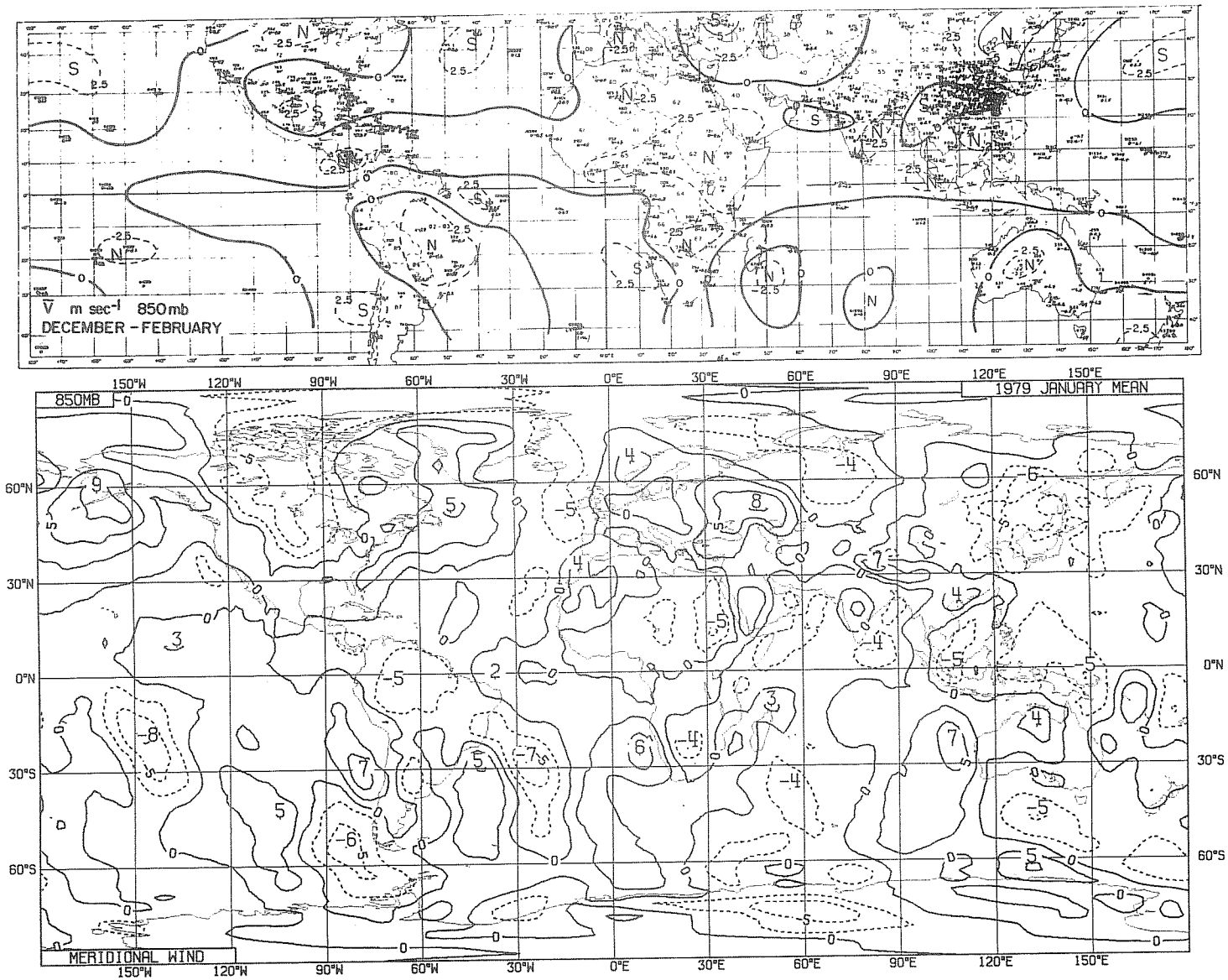

Fig. 7 Same as Fig. 6 but meridional wind at 850 mb

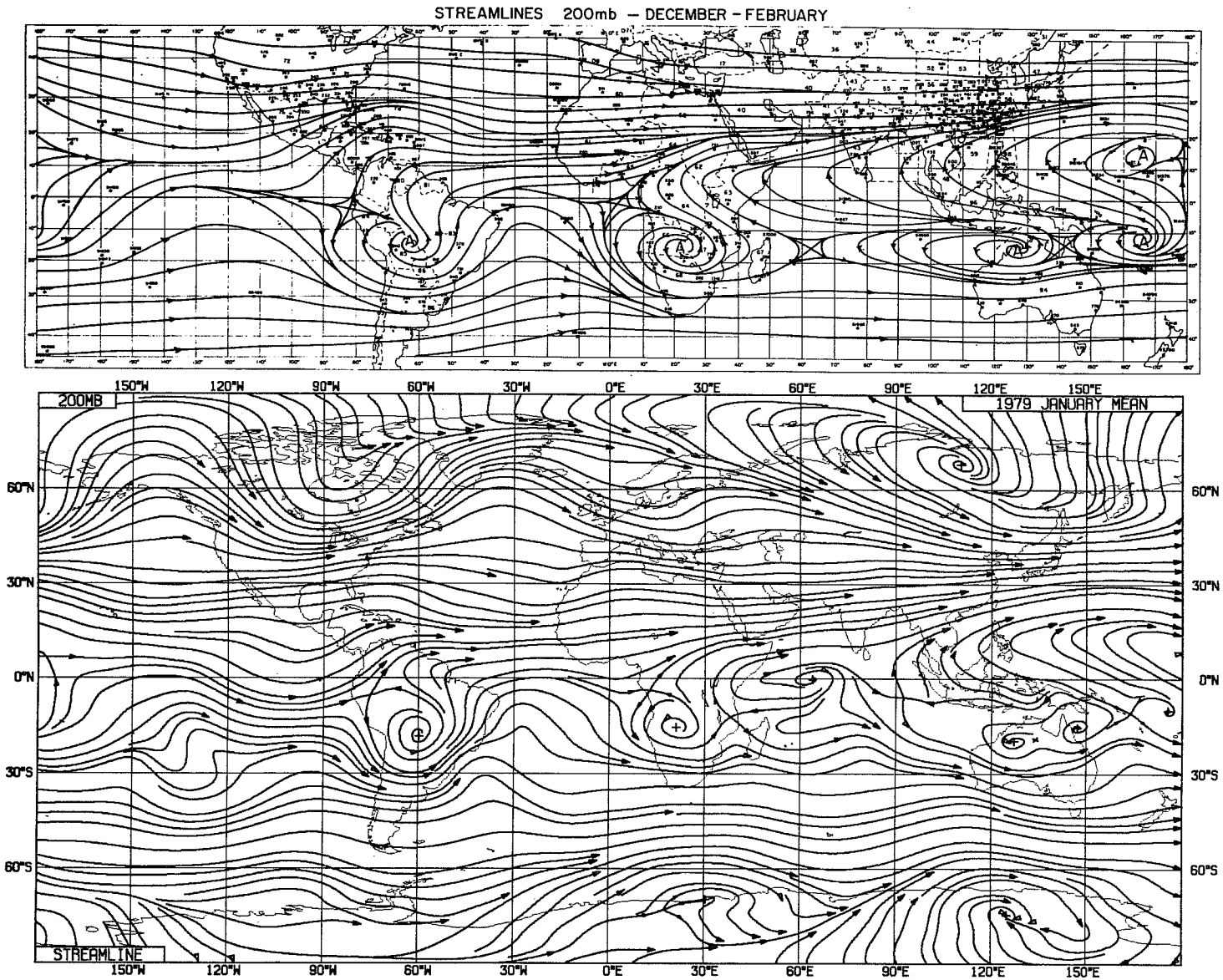

Fig. 8 Same as Fig. 5 but 200 mb

For the zonal winds (Fig. 9), the area of easterlies in the tropics is somewhat smaller in the ECMWF analysis and mostly located over the continents (corresponding to the northern part of anticyclonic vortices located over the continents). The magnitudes are smaller than in Newell's analysis. The pattern over the south-eastern Pacific shows interesting detail with weak easterlies at 30^{o}S, a westerly jet at 15^{o}S (corresponds to the trough extending from Mexico), and a weak westerly zone at 10^{o}N separating the jet from the subtropical jet at 30^{o}N.

Meridional winds (Fig. 10) at 200 mb are 2-3 times larger than in Newell's analysis, and differences are again large over the southern hemisphere ocean areas. Two zones (tilted from southwest to north east) of southerly cross-equatorial flow exist off the west and east coast of South America. Very strong cross equatorial southerlies are shown in the movie of infrared cloud imagery during the special observation period over the similar area (Fleming and Bohan, 1980, presented at the International Conference on Preliminary FGGE Data Analysis and Results, Bergen, Norway).

3.4 Zonally averaged zonal motion field

Fig. 11 shows the latitude-height cross section of zonally averaged zonal wind, both for the ECMWF analysis and for Newell's.
In the northern hemisphere, differences between the two are very small. In contrast, the westerly jet in the southern hemisphere is about 8 m/s stronger in the ECMWF analysis and the westerly area extends much higher into the stratosphere.

The tropical easterly belt in the ECMWF analysis is observed only below 600 mb and above 100 mb. The mean zonal wind in the middle to upper troposphere is a weak westerly.

These differences are more likely the results of improved data coverage over the tropics and over the southern hemisphere.

3.5 Time variability of u and v

To examine time variability, standard deviations of wind components from time averages are computed. Only the zonal mean is shown here.

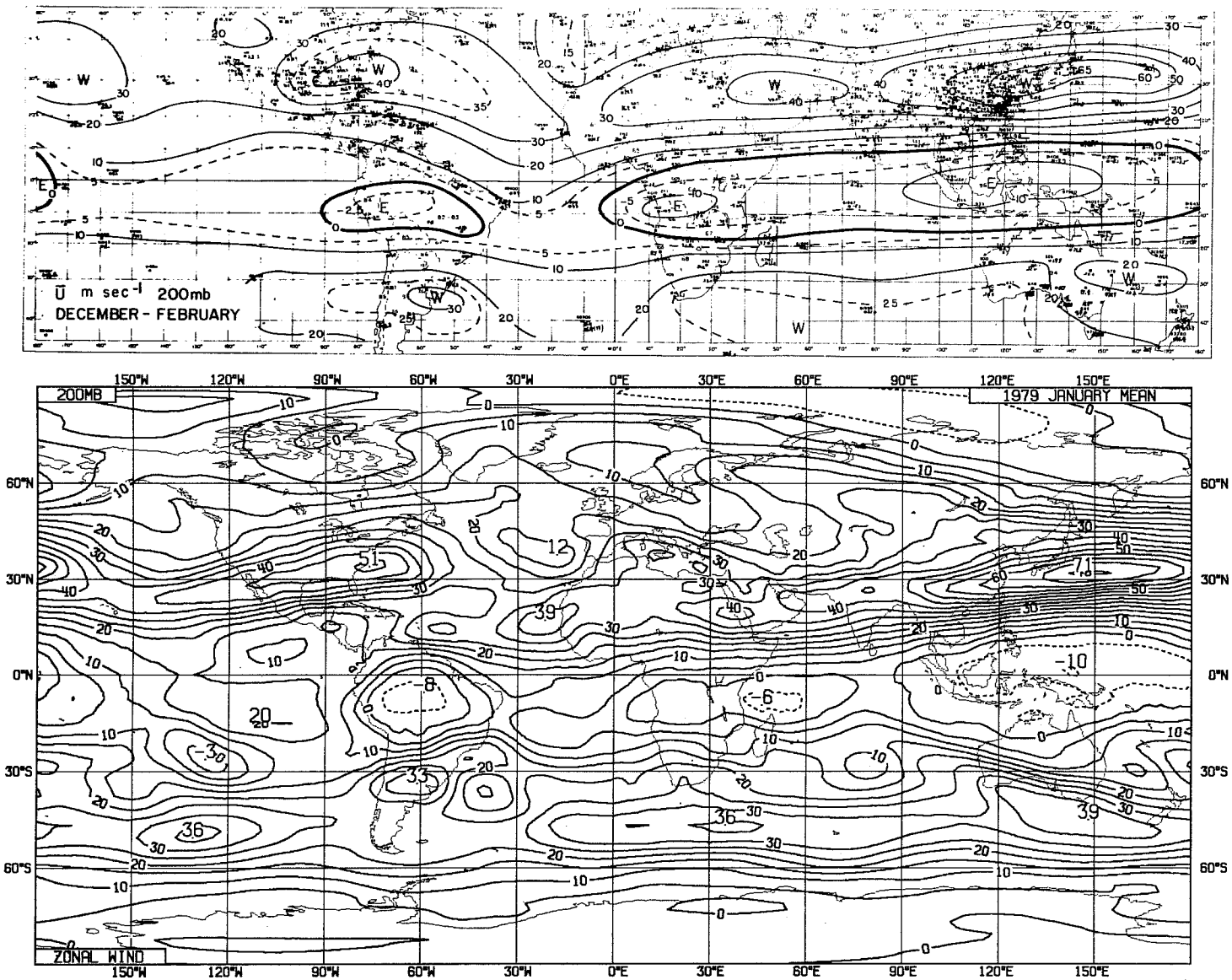

Fig. 9 Same as Fig. 6 but 200 mb, zonal wind, units in m sec^{-1}. Contour interval is 10 m sec^{-1} for Newell's and 5.0 m sec^{-1} for the ECMWF analysis.

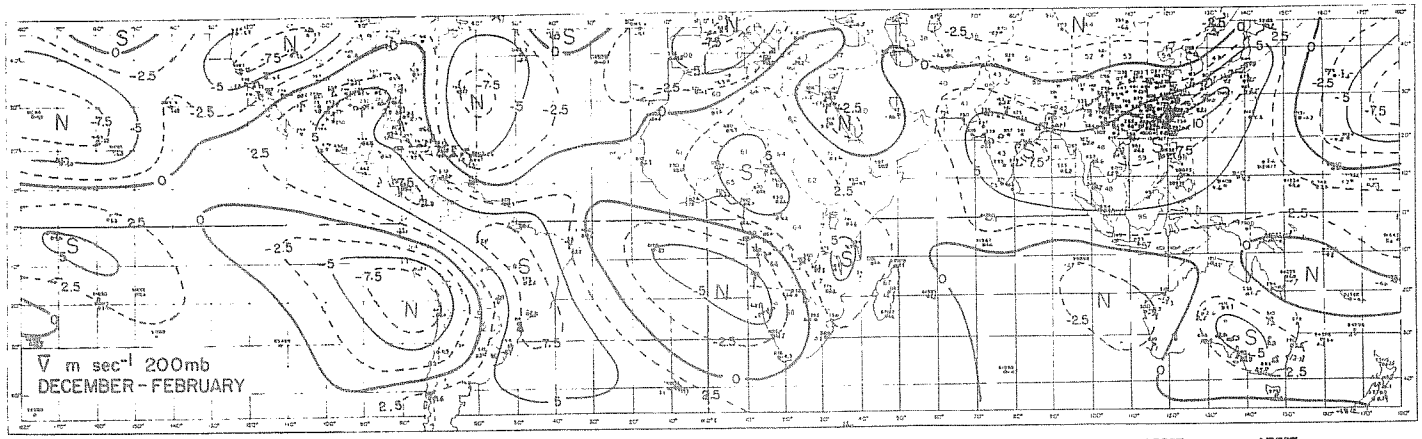

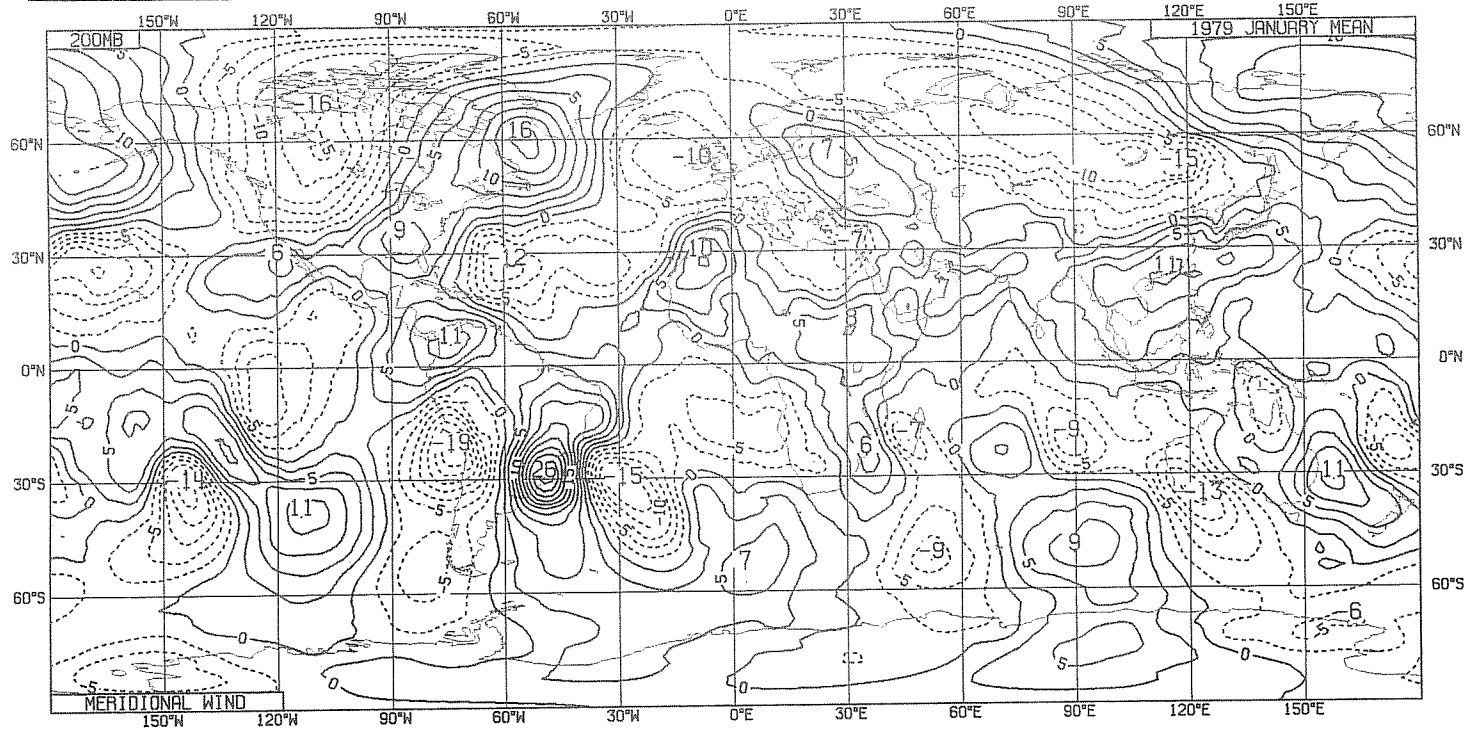

Fig.10 Same as Fig. 7 but 200 mb

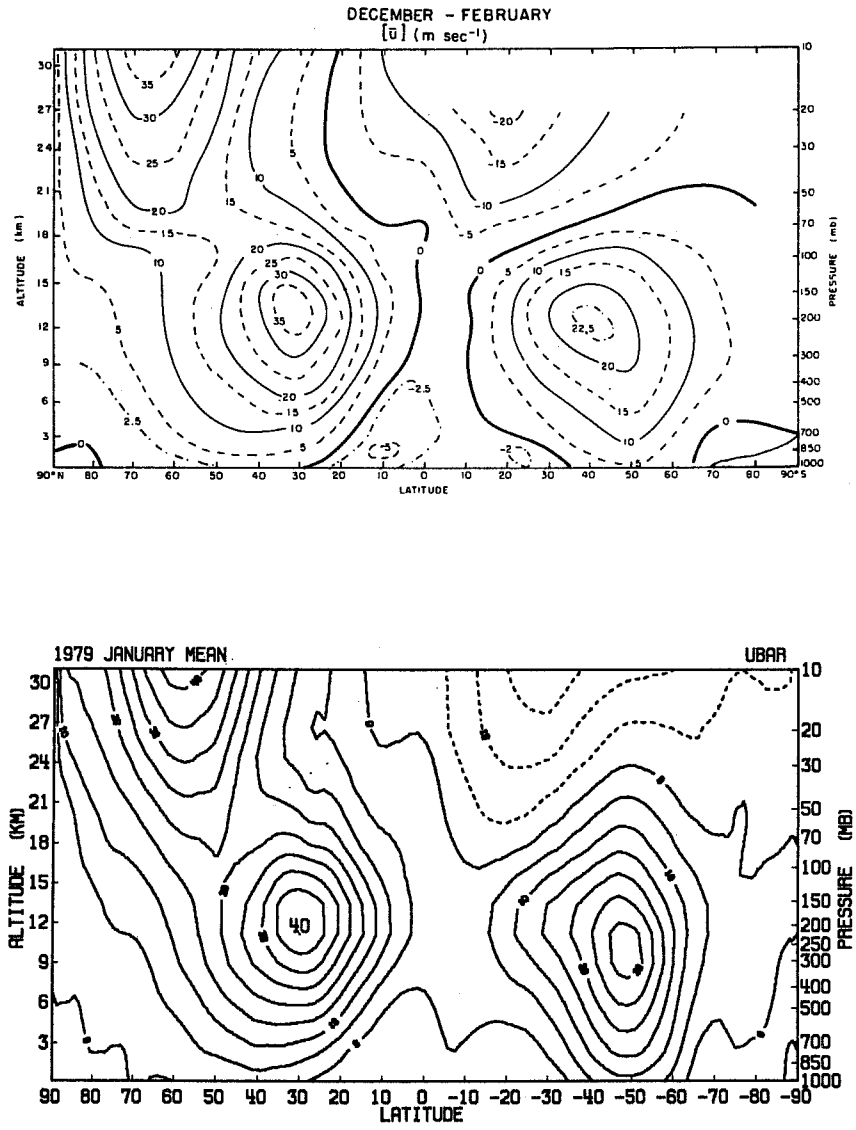

Fig.11 Meridional cross section of the zonally averaged zonal wind. Winter average by Newell et al (top) and January mean from ECMWF analyses (bottom). Units in m sec^{-1}. Contour interval 5 m sec^{-1}.

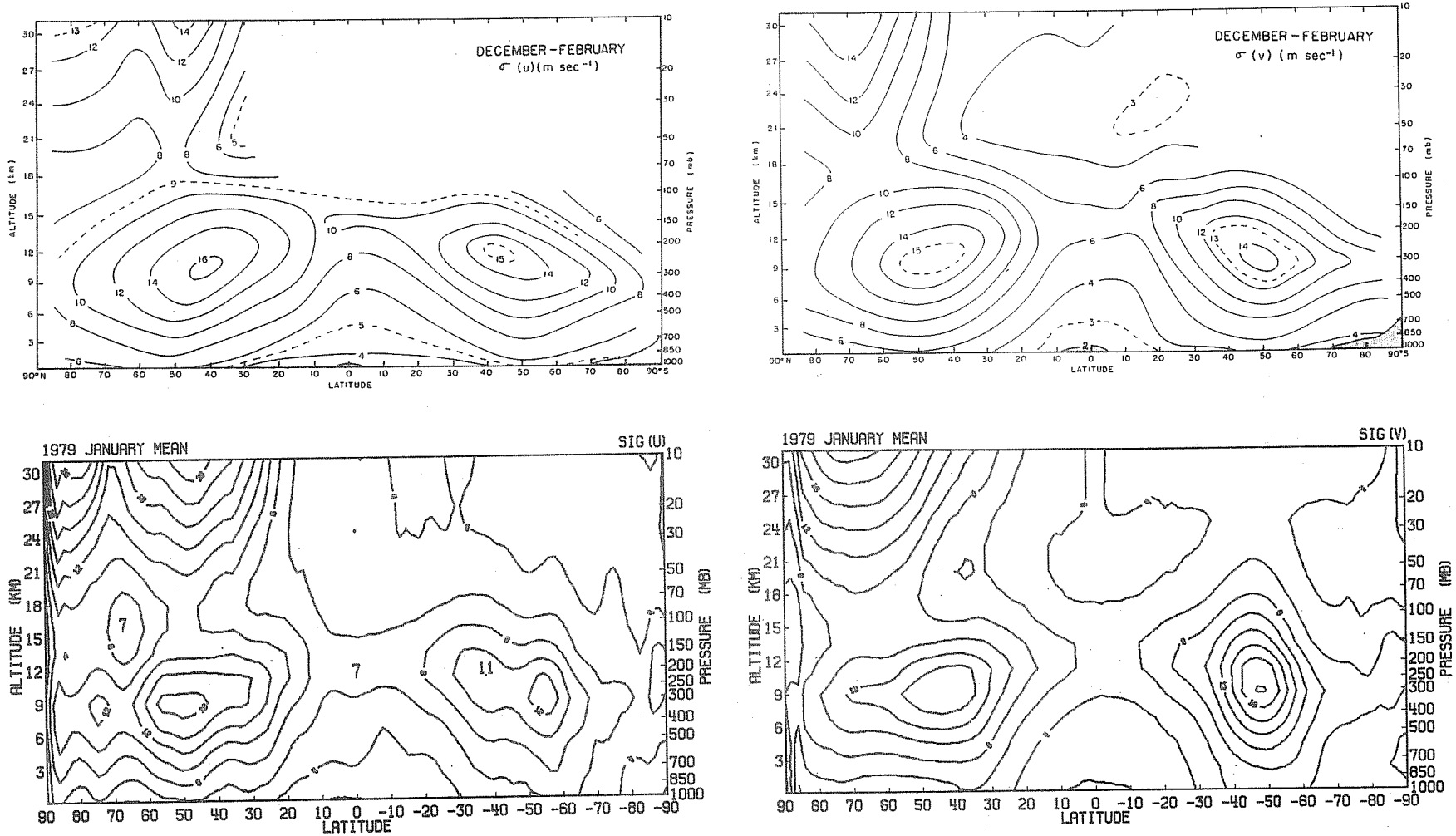

Fig. 12 Same as Fig. 11 but averaged standard deviation of the wind components, u (left) and v (right) from January mean, units in m sec^{-1}. Contour interval is 2 m sec^{-1}.

The standard deviations of u and v (Fig. 12) in the northern hemisphere for the ECMWF and Newell's analyses are again not too different. Large differences are observed in the southern hemisphere where standard deviation of v in the ECMWF analysis is much larger, indicating more aplitude in transient disturbances. On the other hand, time variability of the winds in the tropical upper troposphere is smaller (especially in u-field) in the ECMWF analysis, despite the use of large amounts of cloud wind observations, which are entirely missing in the Newell's analysis. The cause of this smaller variability is not clear at this stage but it can be related to the difference in the types of observations, year to year variations, and in the analysis methods used.

3.6 Momentum transport

Following Newell's analysis, zonal mean momentum fluxes are computed for the ECMWF analysis. The transport is separated into three components, i.e.

$$[\overline{uv}] = [\bar{u}]\,[\bar{v}] + [\bar{u}^*\,\bar{v}^*] + [\overline{u'v'}] \qquad (1)$$

The square bracket and over bar stand for the zonal and time average respectively, and star and prime are the deviation from the corresponding means. The three components are named as flux by the mean meridional motion (the first term on the right of Eq. 1), by the standing eddies (2nd term) and by the transient eddies (3rd term).

The momentum fluxes by the mean meridional circulation (Fig.13 left) show similar patterns for the two analyses. The differences are the stronger fluxes in southern hemisphere for the ECMWF analysis, particularly between 40°S and 60°S. The northern hemisphere stratosphere is also quite different. It is noted that in the ECMWF analyses, combinations of persistency and climatology are used as the initial guess for the analyses above 50 mb and no predicted fields are used. Dynamic control of the initial guess field are considered to be somewhat limited in this sense and further evaluation of the analyses seem to be necessary.

The significant difference of the momentum flux by the standing eddies (Fig.13, right) in the northern hemisphere at 60°N may be due to the blocking. It can also be related to the pronounced stratospheric sudden warming events in the second half of January. The northward fluxes at 30°N are similar. Winter to summer hemisphere transport

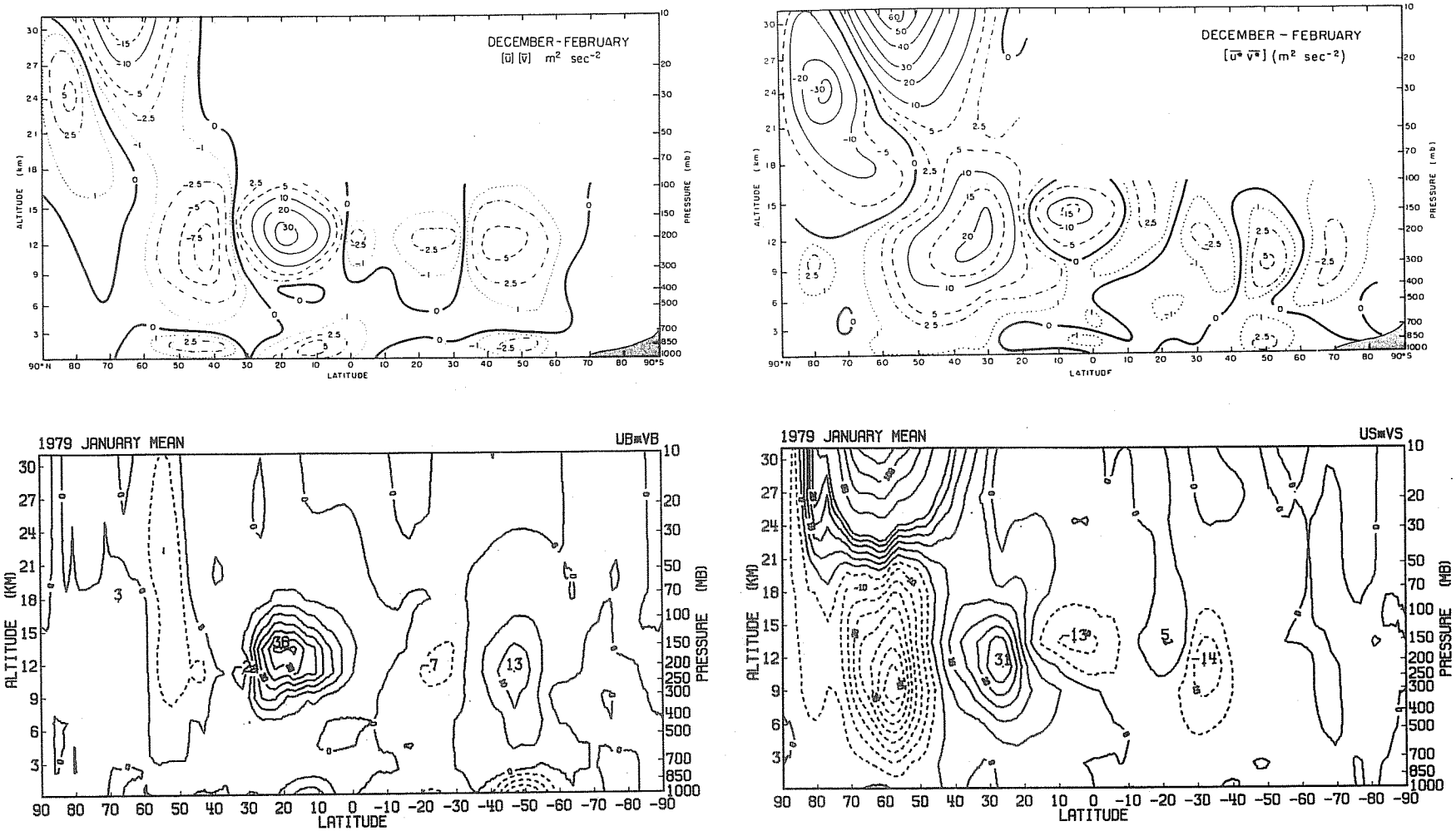

Fig. 13 Same as Fig. 11 but zonally averaged momentum flux by the mean meridional circulation (left) and by the standing eddies (right). Units in m^2 sec^{-2}. Contour interval is 5 m^2 sec^{-2}.

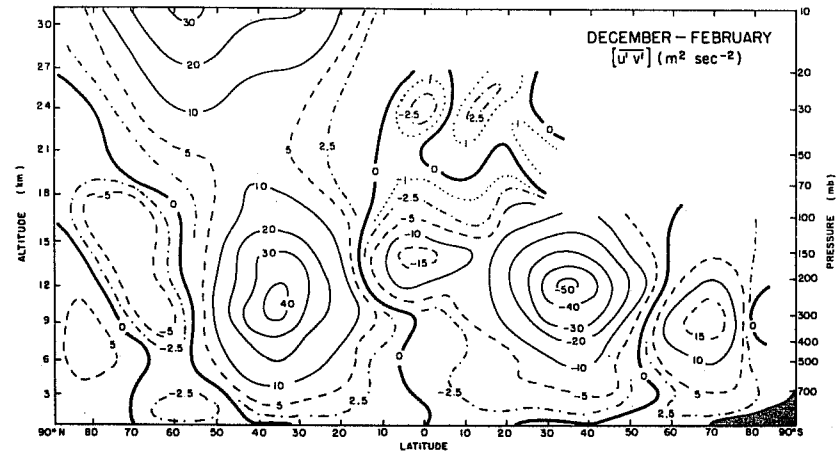

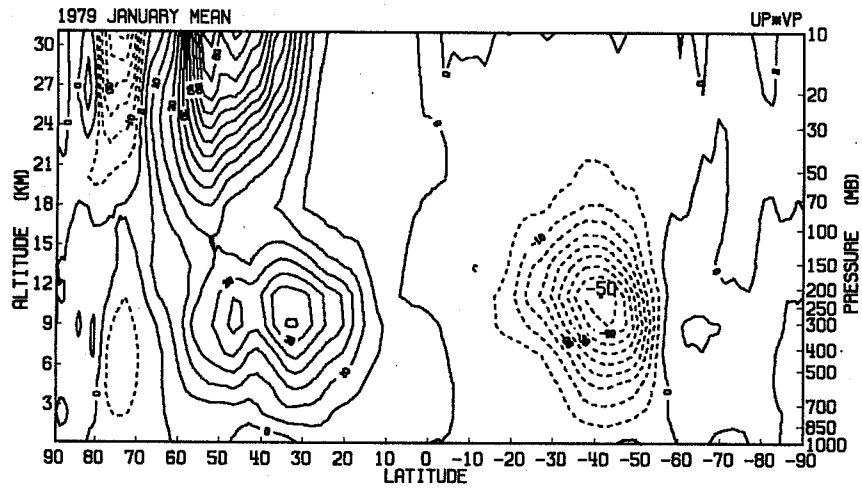

Fig.14 Same as Fig.13 but zonally averaged momentum flux by the transient eddies.

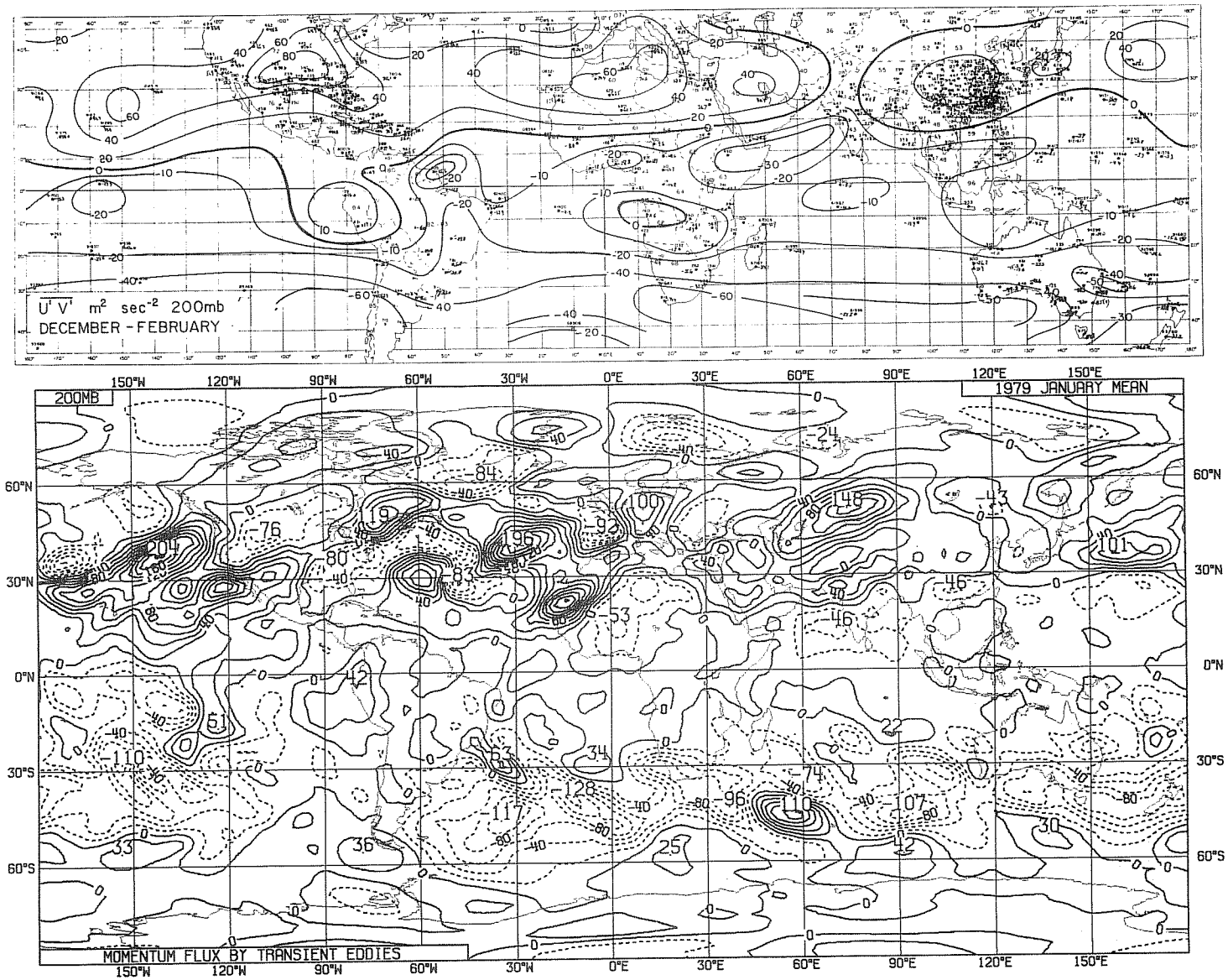

Fig. 15 Horizontal distribution of momentum flux by the transient eddies at 200 mb. Winter mean tropics by Newell et al (top) and January 1979 mean global from ECMWF analyses. Units in m^2 sec^{-2}, contour interval 10 m^2 sec^{-2}.

of momentum at the equatorial upper troposphere exist in both analses, but somewhat weaker in the ECMWF analysis. In the southern hemisphere, southward flux at 30°S stands out in our analysis, but the flux is smaller in other areas, indicating the quite different character of standing waves between the two analyses.

The momentum flux by the transient eddies (Fig.14) shows interesting differences at the equatorial upper troposphere, where the local maximum of southward transport of momentum in Newell's analysis is missing in the ECMWF analysis. To examine the difference of the momentum flux in the tropics, the distributions of $\overline{u'v'}$ at 200 mb are compared (Fig.15). Fair agreement of the signs and magnitudes of the fluxes between the two analyses can be seen in the area where the observations exist in Newell's. Major discrepancies are located over the complete data void area in Newell's analysis (equatorial Atlantic and Pacific). In other areas, the nature of the transient disturbances are alike in the two analyses.

3.7 Divergent part of the wind

In order to examine forcing in the tropics, the velocity potential field has shown to be very useful (Krishnamurti, 1971). The velocity potential (χ) is defined as,

$$\nabla^2\chi = \frac{1}{a\cos\phi}\left(\frac{\partial u}{\partial\lambda} + \frac{\partial v\cos\phi}{\partial\phi}\right) \qquad (2)$$

Here, a is the radius of the earth, ϕ is latitude and λ is longitude. ∇^2 is the Laplacian operator;

$$\nabla^2 = \frac{1}{a^2\cos\phi}\left\{\frac{\partial}{\partial\lambda}\left(\frac{1}{\cos\phi}\frac{\partial}{\partial\lambda}\right) + \frac{\partial}{\partial\phi}\left(\cos\phi\frac{\partial}{\partial\phi}\right)\right\}$$

3.7.1 Analysis and initialization

The analysis scheme used at the ECMWF has two constraints on wind analysis, i.e. geostrophic constraint (relaxed toward the equator) and the local nondivergence of the analysis increment (of the scale less than 600 km). Therefore analyzed divergence is originated from the initial guess divergence and the analyzed divergence of the scale greater than 600 km.

To look at the magnitude of the contributions from the above two sources of divergence, the analysis increment of the velocity potential is computed. Fig. 16 shows an example of the pattern of χ at 200 mb (January 17 12GMT 1979, this date being arbitrarily chosen). The analysis increment (Fig. 17, upper) is as large as or larger than

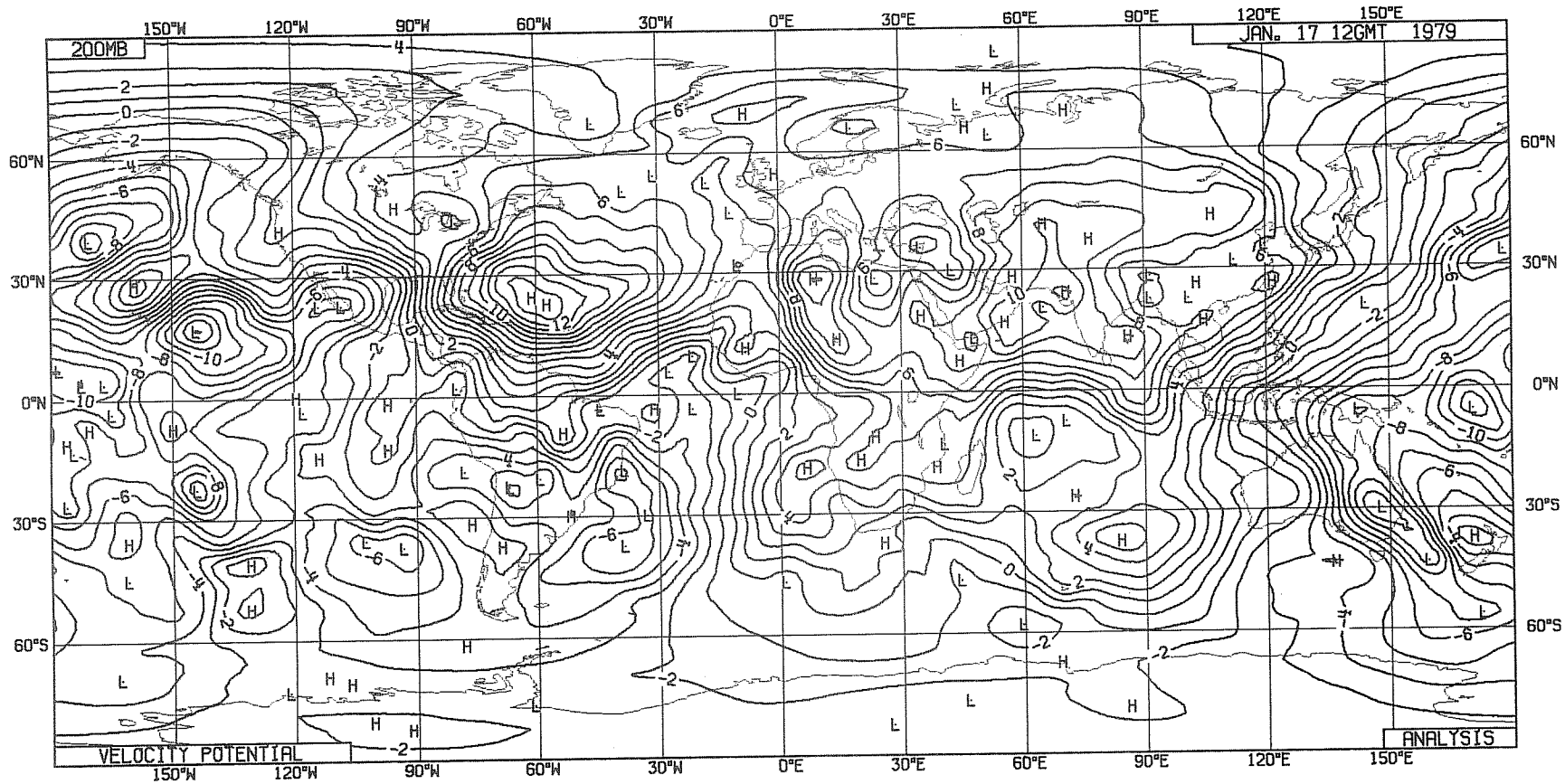

Fig. 16 Velocity potential field at 200 mb computed from uninitialized wind field (January 17 GMT 1979). Units in x 10^6 m^2 sec^{-1}. Contour interval is 10^6 m^2 sec^{-1}.

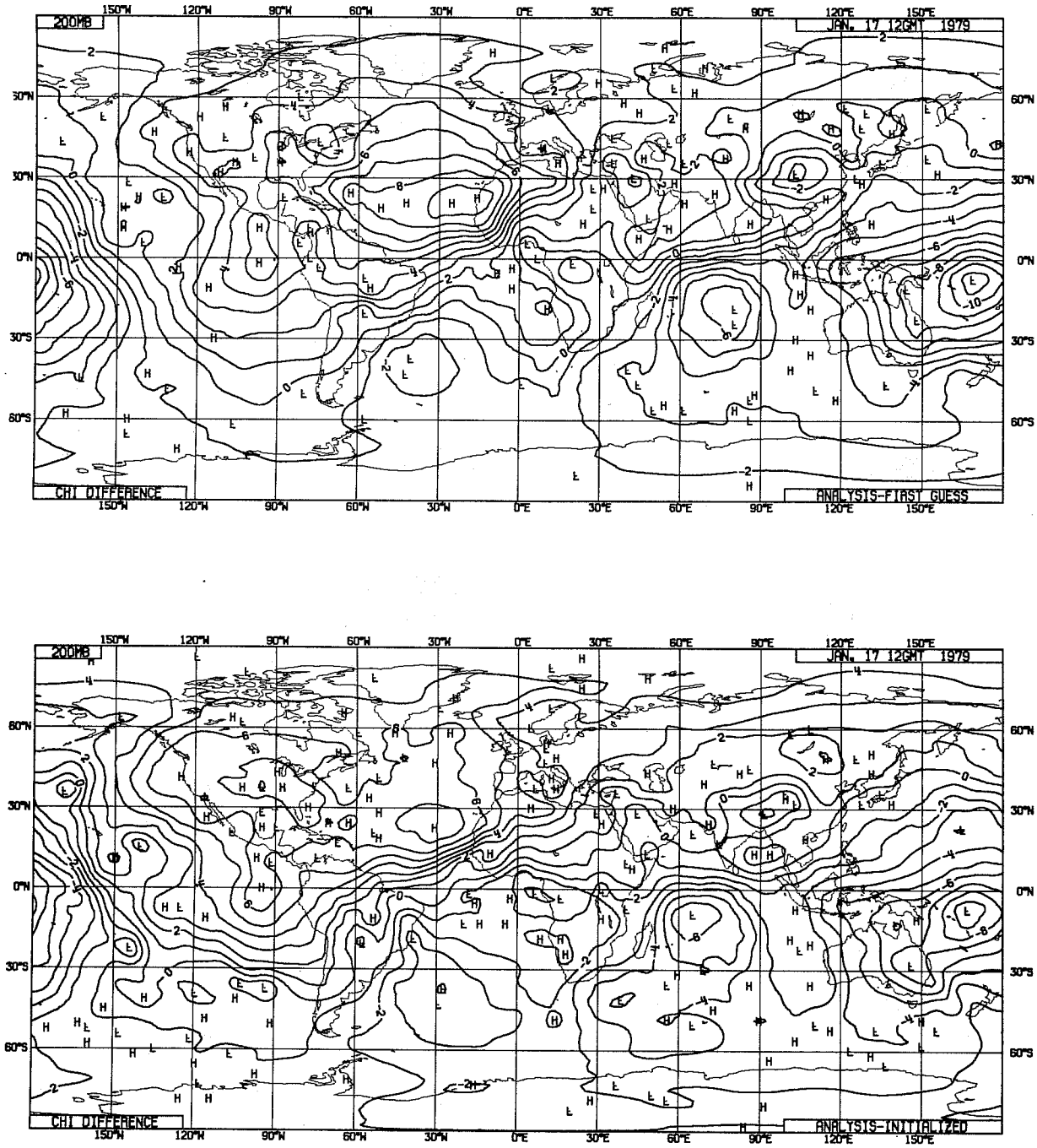

Fig. 17 Difference of velocity potential between the analysis and initial guess (top) and between the analysis and the initialized field (bottom), units in x 10^6 m^2 sec^{-1}. Contour interval is 10^6 m^2 sec^{-1}.

the analyzed values particularly in low latitudes. In the lower half of Fig. 17, the difference between the analyzed and initialized χ field is presented. It is evident that the initialization procedure removes low latitude large scale divergences. The main reason for this reduction seems to be due to the lack of diabatic heating in the initialization. Furthermore, the first guess field which is the six hour prediction with full physics from previous analysis fails to recover the proper magnitude of divergence in low latitudes. This problem seems to be related to the slow build up of diabatic heating (mainly latent heating) in the prediction model.

The main reason for the use of uninitialized fields throughout this study is based on the above examination of the divergence field. It is noted that in high latitudes the effect of the initialization is much smaller due to the fact that the divergence is controlled mainly by the dynamics rather than by the diabatic heating.

3.7.2 January mean velocity potential field

Fig. 18 (upper panel) shows the mean χ-field at 200 mb during January 1979. A marked minimum is located at 15^{o}S, 175^{o}E. Two other areas of minimum are noted over South America and southern Africa, corresponding to the areas of climatologically active convection (and also corresponding to the anticyclonic circulations in flow field as shown in Fig. 8). Three maxima are located in each hemisphere, corresponding roughly to the surface high pressure areas (see Fig. 1 and 3).

The divergent component of the wind is defined as

$$u_{\chi} = \frac{1}{a \cos\phi} \frac{\partial \chi}{\partial \lambda}$$

$$v_{\chi} = \frac{1}{a} \frac{\partial \chi}{\partial \phi} \quad , \qquad (3)$$

the wind vector directing from χ minimum to maximum. The vertical circulations expected from the distribution of χ are the three local Hadley circulations located at around 120-150^{o}E, 30^{o}E and 60^{o}W, strongest circulation being the first one with rising over the southwestern Pacific and sinking over Siberia. In the southern hemisphere, circulations in east-west are more evident, all of them rising over the continent and sinking over the ocean. The velocity potential pattern at 850 mb (Fig. 18, lower panel) shows good

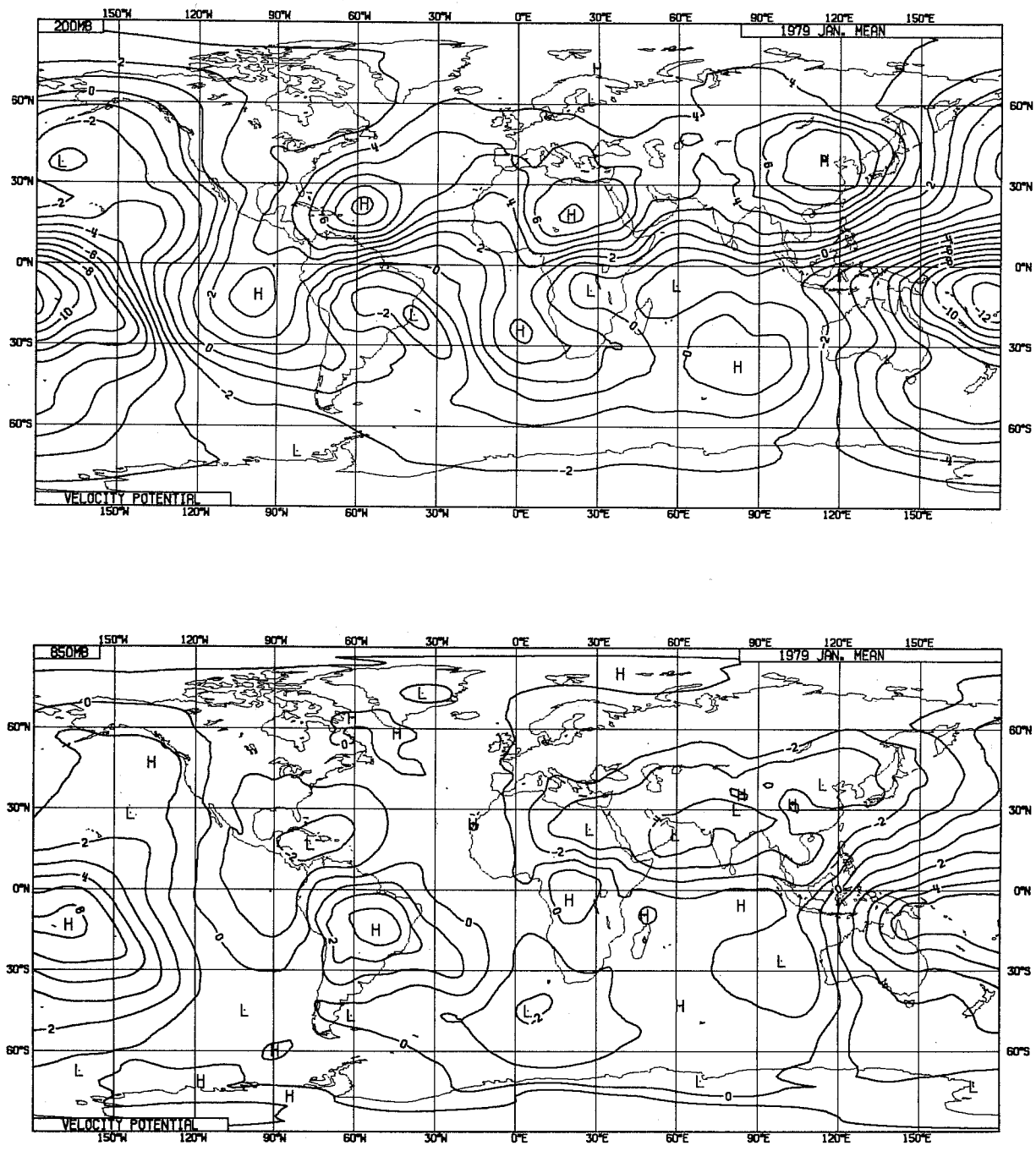

Fig. 18 January 1979 mean velocity potential field 200 mb (top) and 850 mb (bottom). Units in x 10^6 m^2 sec^{-1}. Contour interval is 10^6 m^2 sec^{-1}.

negative correlations with 200 mb, supporting the existence of above vertical circulations. Considering that the analysis does not have any constraints on the vertical distributions of divergence except through the initial guess field, it is remarkable that the analysis scheme and the data (mostly cloud winds from satellites) can produce such a consistent velocity potential field.

3.7.3 Validity of the analysis

The velocity potential field during northern hemisphere winter is presented by Krishnamurti et al (1974). Their computation is based on the analysis during December 1969 by the U.S. National Meteorological Center. The general pattern of the velocity potential agrees with the FGGE analysis but some of the details are quite different. This comparison is not conclusive since the NMC analyses are based on poor data coverage in the tropics with no cloud motion vectors.

For better qualification of the analysis of the divergence field, some measure of convective activity is helpful. This is performed by Julian using archived satellite infrared digitized data at the National Center for Atmospheric Research. The details are reported elsewhere in this report. His study shows that the agreement of velocity potential minima and convective activity are remarkable in the monthly average and even in the daily chart.

This fact provides good basis for the validity of the divergence analysis at least from a qualitative point of view.

3.7.4 Vertical distribution of the divergent part of wind

The distributions of velocity potential in the vertical have not been performed before simply because proper observations were not available especially in the lower to middle troposphere.

To exhibit the vertical distributions in a physical way, the kinetic energy of the divergent part of the wind is computed. Then, the divergent kinetic energy is further separated into u-energy and v-energy, i.e.

$$K_{u\chi} = \frac{u_\chi^2}{2}$$

$$K_{v\chi} = \frac{v_\chi^2}{2} \qquad (4)$$

$K_{u\chi}$ and $K_{v\chi}$ are the measure of the strength of the east-west and the local Hadley circulations, respectively. Furthermore, each kinetic energy is expressed in terms of zonal Fourier component to separate the space scales.

We present in Figs. 19 and 20 only two wave components (wavenumber 1 and 3), which have larger magnitude than other scales. In general, divergent kinetic energy is very small compared to the total kinetic energy (less than 5%). However, they are very important since all the conversion from potential (available) energy to kinetic energy takes place via the divergent part of the wind (Chen and Wiin-Nielsen, 1976). The large divergent kinetic energy is confined near the tropopause, in the boundary layer (below 850 mb) and in the northern hemisphere stratosphere. An interesting character of the divergent kinetic energy is that the u-energy tends to have fairly large north south scale, while v-kinetic energy is concentrated in relatively narrow latitudinal bands (10^{o} - 15^{o}). This is very clear in the u-energy of zonal wavenumber 1, which has the scale of the distance between the two poles. (This is also confirmed in the successive February mean). There is some agreement of the location of the maximum of total kinetic energy and divergent v-kinetic energy in wavenumber 1, at 10^{o}N, suggesting conversion of potential to kinetic energy on this scale. Zonal wavenumber 3 indicates the existence of the east-west circulations at 10^{o}S. The $K_{u\chi}$ maximum is situated at the middle of two maxima of $K_{v\chi}$ showing a very narrow zone of forcing at 10^{o}S.

4. KINETIC ENERGY BUDGET IN WAVENUMBER DOMAIN

We have examined several January averaged quantities of the ECMWF analysis against available corresponding climatologies in Section 3. From this examination, we are able to conclude that the analyses are of good quality from a long time averaged point of view.

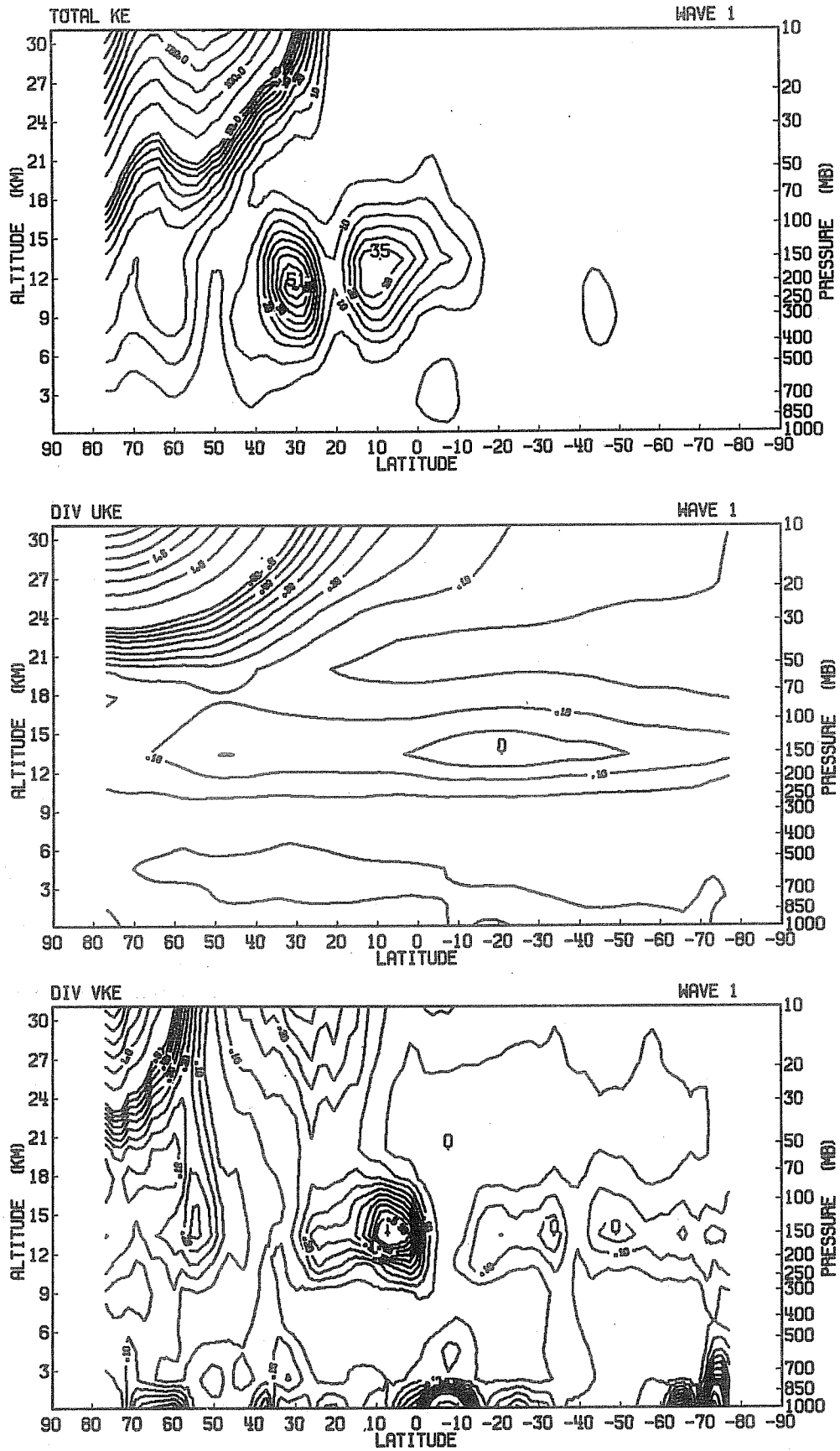

Fig.19 Meridional cross sections of the total kinetic energy (top) divergent u-kinetic energy (middle) and divergent v-kinetic energy (bottom) for zonal wavenumber 1, unit in $m^2\ sec^{-2}$. Contour interval is 5 $m^2\ sec^{-2}$ for the total kinetic energy (25 $m^2\ sec^{-2}$ for values greater than 50 $m^2\ sec^{-2}$) 0.05 $m^2\ sec^{-2}$ for the divergent kinetic energies (0.25 $m^2\ sec^{-2}$ for the values greater than 0.5 $m^2\ sec^{-2}$). The contours poleward of 80^oN and 80^oS are suppressed to prevent excessive crowding of the contours.

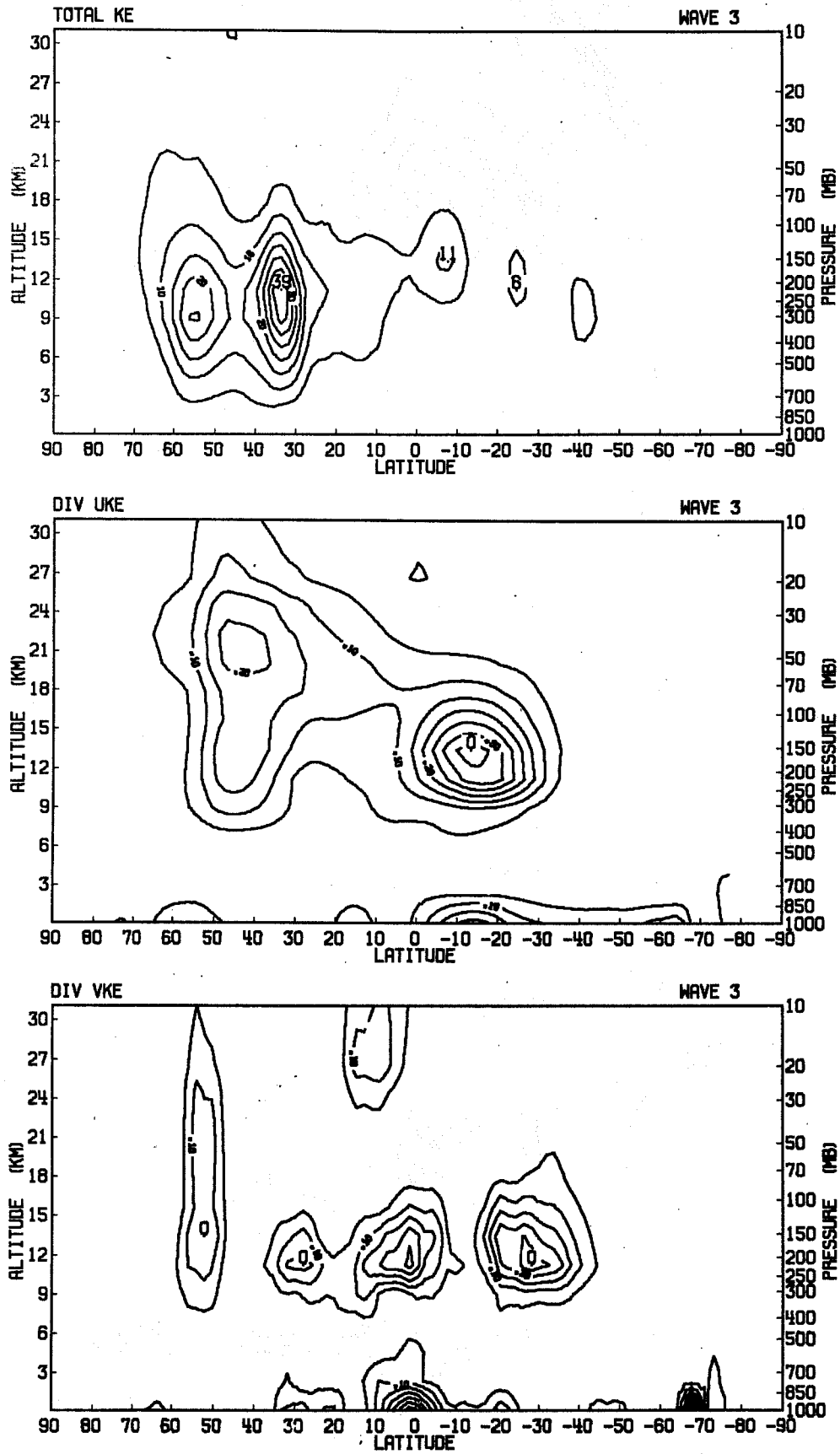

Fig.20 Same as Fig.19 but for zonal wavenumber 3.

In this Section, we discuss kinetic energy budget calculations applied to the ECMWF analysis. Two major objectives can be noted. One is to examine further the physical consistency of the analyses, and the other to look into the energetics of the atmosphere in some detail.

4.1 Separation of scales

In formulating energy budget equations, there are several methods to separate space scales of the motion field. Decomposition into the zonal averages and the deviations from them is practical and commonly applied (e.g. Oort, 1964), but it cannot reveal the different energetical nature of the very large scales and smaller scales which are known to be quite different. The space scale can be expressed either by the zonal Fourier coefficients at each latitude or by the spherical harmonic coefficients. The spherical harmonic analysis is very attractive from a mathematical point of view and also for describing the statistical character of the transient disturbances (Baer, 1972). However, it seems to have some weakness when applied to the atmosphere, which has large inhomogenuity in the long time averages. Table 1 shows spherical harmonic spectra* of the mean FGGE January analysis at 200 mb.

---

* Only rotational part of the winds are considered. The spherical harmonic component of the kinetic energy is expressed as

$$K_{\ell}^{m} = \frac{\ell(\ell+1)}{2a^2} (2-\delta_{om}) \left|\psi_{\ell}^{m}\right|^2 ,$$

where δ_{om} is a delta function, $\delta_{om} = 1$ for $m = o$ and $\delta_{om} = o$ for $m \neq o$, and ψ is a streamfunction defined as

$$\nabla^2\psi = \frac{1}{a \cos\phi} \left\{ \frac{\partial v}{\partial \lambda} - \frac{\partial}{\partial \phi} (u \cos\phi) \right\}$$

It is noted that the contribution of the divergent part of the wind to the total kinetic energy is very small as has been discussed in Sect. 3.7.4.

Table 1. Spherical harmonic kinetic energy spectra of the rotational part of the wind at 200 mb for 1979 January mean analysis. The numbers in each column indicate energies for the given zonal wavenumber index (m) with increasing value of ℓ-m from bottom to top, ℓ being the order of the Legendre polynomial. Units are in m^2 sec^{-2}. Only the values for $1 \leq m \leq 7$ and $0 \leq \ell - m \leq 7$ are shown.

ℓ-m	m=1	m=2	m=3	m=4	m=5	m=6	m=7
7	1.1	0.9	1.3	0.3	0.0	0.0	0.0
6	7.9	0.1	1.8	1.0	0.0	0.0	0.1
5	3.8	0.4	1.4	0.5	0.2	0.0	0.1
4	0.2	3.3	2.1	2.4	0.4	0.1	0.1
3	10.1	6.9	6.3	2.6	0.8	0.1	0.4
2	1.3	0.5	0.3	0.4	0.7	0.6	0.6
1	0.3	0.7	1.1	0.5	1.8	1.9	0.6
0	0.0	0.1	0.1	0.2	0.0	0.2	0.2

The energy spectra spreads in many spherical harmonic components and it is very difficult to see systematic distributions in zonal wavenumber index (m) nor in the degree of the Legendre polynomial (ℓ). There is a fair indication that the kinetic energy peaks appear in the components of odd values of ℓ-m showing dominance of anti symmetric mode with respect to the equator). This broad spectra of the monthly means discourages us from using spherical harmonic decomposition. Hence, we have decided to use zonal Fourier decomposition, and tried to examine the latitudinal variations. The zonal Fourier decomposition has an advantage that the dominant mode can be easily identified in the original field, the disadvantage being the variation of actual wave lengths with latitude for the same wave number.

4.2 The energy budget equations in wavenumber domain and the computational method

The equations of energetics in wavenumber domain was first derived by Saltzman (1957). The temporal change of the wave components of kinetic energy at any latitude are written as follows.

$$\frac{\partial K(o)}{\partial t} = \sum_{m=1}^{\infty} M(m) + C(o) + F(o) + W(o) + D(o) \tag{5}$$

$$\frac{\partial K(m)}{\partial t} = - M(m) + L(m) + C(m) + F(m) + W(m) + D(m)$$

In the above equations, K(m) is the kinetic energy of wavenumber m, m = o being zonal average, M is energy exchange between the zonal motion and the waves, C is the conversion from available potential energy, L is the kinetic energy exchanges between the waves, F is the boundary flux convergence both in the horizontal and in the vertical, W is the pressure work at the boundaries and D is dissipation. The complete forms of the energy conversion terms on the right hand side of Eq.(5) are described in the Appendix.

The energy conversion terms are evaluated in the box surrounded by the grid points between the two standard pressure levels (Fig. 21). As can be seen in the Appendix, the conversion terms consist of several pairs of terms related by the continuity equation. Finite differences in the north-south and in the vertical require some caution to avoid any fictitious generation of mass and energy, which causes serious errors in the evaluation of some of the terms. The grid

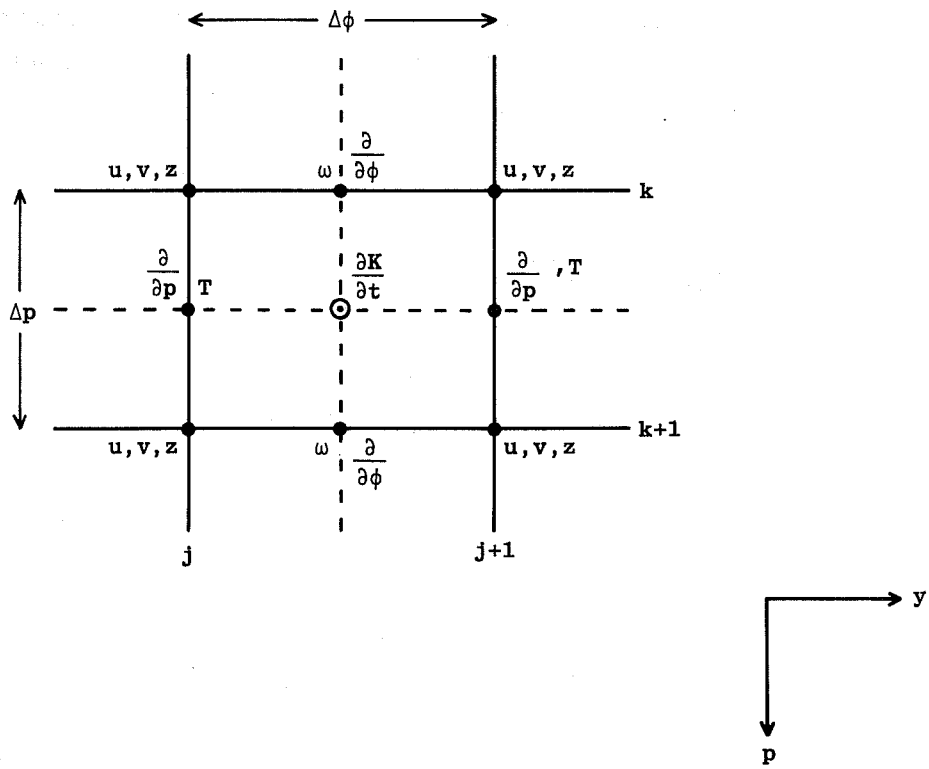

Fig.21 Configuration of grids used in energy budget calculations. j denotes index for the north-south grids and k for the pressure levels.

system (Fig. 21) is chosen for this reason.

The temperature is computed from the thickness between the two pressure levels. No vertical interpolation is involved. The vertical velocity (ω) is computed from analyzed (uninitialized) u and v assuming ω = o at 1000 mb. No constraint on ω is applied in the calculation. Moreover, no particular care is taken over the high topography area (u,v and z are analyzed even if the pressure surface is below the ground). The upper limit of the wavenumber is set to 30 in all the calculations.

The dissipation terms are computed as residuals knowing the time tendency of the kinetic energy from the analyses 12 hour apart. This residual was found to be as large as other terms even in the monthly average, with both negative and positive signs. This suggests uncertainties in evaluating some of the conversion terms due to time and space truncation errors (including the effect of waves shorter than wavenumber 30), and to the physically inconsistent analysis. To find the terms responsible for these uncertainties in the evaluations of the conversion terms, 12 hourly values of each term are mapped and checked particularly when the residuals become large positive. It was found, in most cases, that the terms related to the divergence are the source of the problem. This is in fact expected from a somewhat crude way of computing vertical motion as noted earlier. This indicates that although a long time averaged large scale divergence field seems to show very reasonable distributions as discussed before (3.7.2), individual analyses are not accurate enough in magnitude and in the correlation with other variables to give reasonable estimates of the energy conversions. To overcome these problems, use of initialized vertical motion is very attractive but still not adequate in low latitudes (see 3.7.1). Thus, since it is not so simple to obtain accurate vertical motion fields, we have decided to eliminate all the terms related to the divergence (terms with ω as well as the pressure work term at the boundaries which relates to the divergent part of the wind) and included them in the residual term. This implies that in Eqn. 5, part of the terms, M,L and F (terms related to the vertical advections), and the terms C, W are combined with the term D (see Appendix).

4.3 Kinetic energy budget during January 1979

In order to examine the energetics in the tropics as well as in high latitudes, we have selected the layer between 250 mb and 200 mb, where tropical activity is greatest (see Figs. 12-14, 19-20). Fig. 22 shows energy diagrams for the northern hemisphere ($90^{o}N$ - $20^{o}N$), tropics ($20^{o}N$ - $20^{o}S$) and for the southern hemisphere ($20^{o}S$ - $90^{o}S$).

4.3.1 Northern hemisphere (Fig. 22, left)

In the northern hemisphere, zonal-wave interactions (M) are smaller than the wave-wave interactions (L). The zonal motion receives kinetic energy from waves as a total (some waves receive energy from the zonal but not significantly). The wave-wave interaction shows a large output of energy from baroclinic waves (wavenumber, m = 7 to 10) to long (particularly wavenumber 1) and short waves (with some exceptions). The residual terms indicate input of energy to baroclinic waves suggesting conversion from potential energy to kinetic energy in this scale. A large output of kinetic energy in wavenumbers 1 and 2 is noted. The overall energy exchanges are in very good agreement (although details are not quite the same) with similar studies performed by various people, which are summarized by Saltzman (1970).

4.3.2 Southern hemisphere (Fig. 22, right)

The most striking difference from the northern hemisphere is that the zonal-wave interaction is larger than the wave-wave interactions. This is physically quite convincing since the ultralong waves in the southern hemisphere are not as active as in the northern hemisphere due to the weaker forcing by surface irregularities. This also suggests the importance of surface conditions in generating and maintaining the ultralong waves.

Zonal wave interactions are much simpler than in the northern hemisphere. All the waves supply energy to the zonal motion, peaking at m = 5 (the dominance of which has been noted in Fig. 4). Wave-wave exchanges are not so simple but in general, conversions from baroclinic waves (m = 7 to 10) to other waves are taking place.

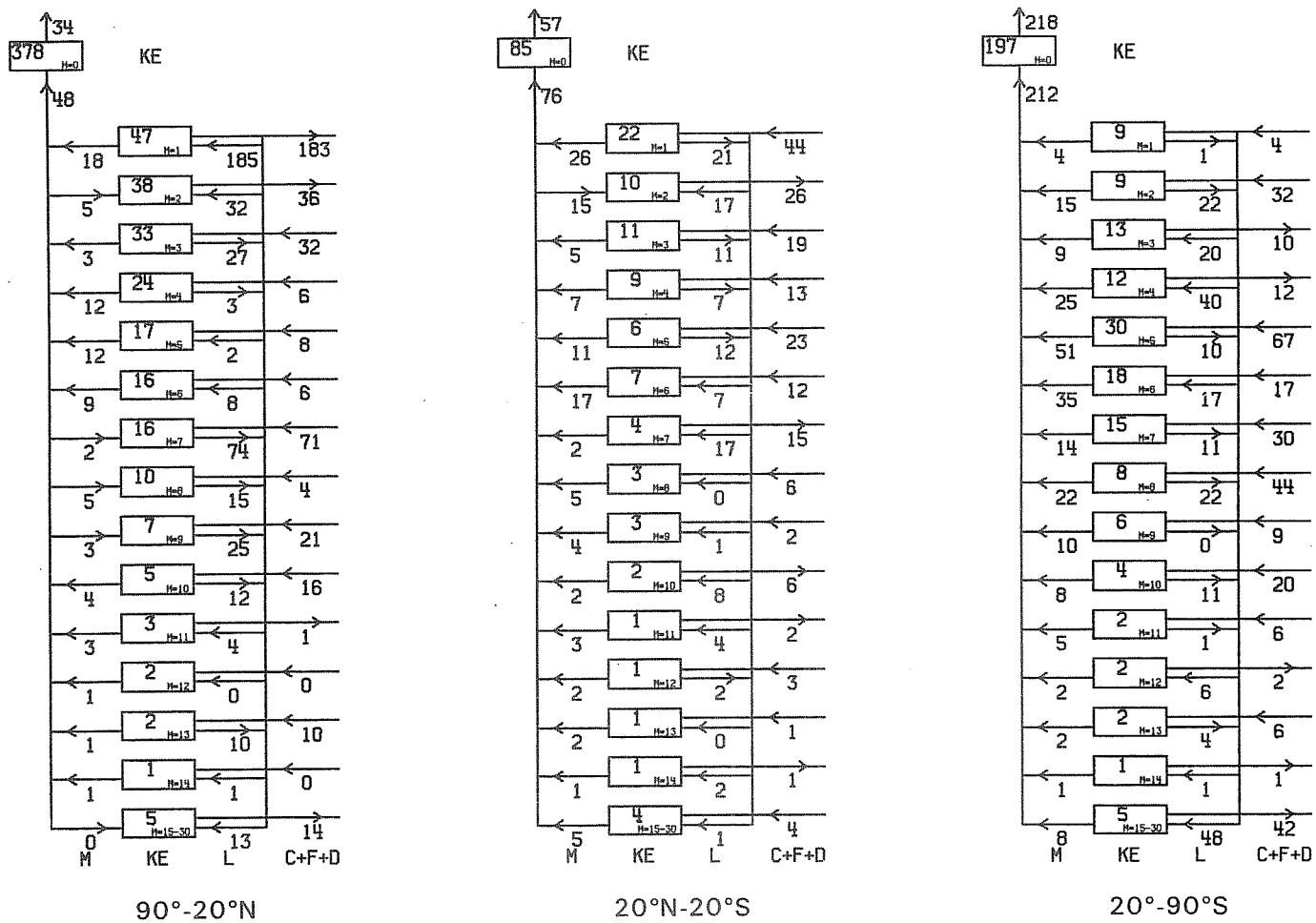

Fig. 22 Energy diagram for the northern hemisphere (left) tropics (centre) and southern hemisphere (right) in the layer between 200 and 250 mb during January 1979 obtained from ECMWF anlyses. The large numbers in the boxes are the area averaged kinetic energies of the zonal Fourier component m indicated by the small number. The box at the top of the diagram is for the zonal mean field (m=o). The arrows and lines at the left side of the diagram connecting the boxes with the one at the top indicate zonal-wave interactions (M) and their directions. Similarly the lines connecting the boxes on the right side of the diagram indicate wave-wave exchanges (L). The other lines on the right and at the top indicate the residuals (the sum of conversion from potential energy, boundary fluxes, dissipations, etc). Units are in m^2 sec^{-2} for energies, m^2 sec^{-3} for the conversions.

4.3.3 Tropics (Fig. 22, centre)

The tropical energetics is quite different from those in high latitudes. The energy spectrum is more simple having its maximum at m=1 and decreasing nearly monotonically as scale decreases (the number in the boxes of Fig.23 is the energy of each wave in $m^2 sec^{-2}$ unit). This is considered to be due to the weak baroclinic wave activity in the tropics. The zonal motion (weak westerlies, ~ 13 m/s) is maintained by the waves (except by m = 2). The sources of kinetic energy for smaller scales ($m \geqslant 6$) are the ultralong waves (m = 1, 3 to 5) which are maintained by C+F+D, most likely by the conversion from potential energy suggested in Figs. 16, 20 and 21. The energy conversion to medium scale waves (m = 7 to 11) suggests development of waves by barotropic instability.

In summary, most essential differences of energetics in the three regions selected above can be summarized as follows.

i) Major kinetic energy source in high latitudes is in the baroclinic waves

ii) In the northern hemisphere, this energy source is used mainly to maintain ultralong waves

iii) In the southern hemisphere, it is used to maintain the zonal motion

iv) Major kinetic energy source in the tropics is the ultralong waves forced by the organized tropical convection (and probably by the middle latitudes).

It is noted that the tropical energetics obtained here does not quite agree with the one by Krishnamurti et al (1973) in the conversion between the zonal and the ultralong waves (m = 1 to 3 receive energy from the zonal in their study). We have repeated the calculations by taking the same domain as Krishnamurti's ($15^{o}N$ - $15^{o}S$). In this domain, m = 1 still provides energy to the zonal but less in magnitude (15 units vs 26 units). The m = 3 and zonal conversion reversed in sign (m = 3 receives 5 units). Since the differences between the two studies can be due to various other reasons (month to month, year to year change, data coverage etc.), we have not tried to examine this discrepancy further.

4.4 Latitudinal variation of the energetics

There are two major reasons to examine latitudinal variations of the energetics. One is to understand the somewhat complex nature of the ultralong waves in the northern hemisphere (Fig. 22) and the other is to look into the cause of the differences in detail of the energetics among various studies, some of which are noted in the previous section.

Fig. 23 shows latitude-time variations of the kinetic energy of m = 1 at 200 mb. The most apparent character of the wave is the very narrow north-south scales (about 10^{o} from minimum to minimum) with maximum at around 10, 30 and 60^{o}N. Tropical wavenumber 1 has somewhat larger scale. The small N-S scale agrees with the synoptic observations of the narrowness of the local westerly jet. Similar figures for other waves (not shown) indicate that m = 2 also has narrow N-S scale, but as m increases, there is a tendency that the N-S scale increases. For the baroclinic waves (m=7-10) the N-S scales are 20-30^{o} latitude from minimum to minimum. The small N-S scales of the ultralong waves suggest large latitudinal variations of the energetics in this scale.

Another noteworthy feature of the ultralong waves are their temporal variations. The kinetic energy of m = 1 at 30^{o}N, for example, goes through considerable variations from very intense state (Jan 1 - 7) to almost non existent (Jan 23-27). Similar large variations (not so clearly coherent with other waves) are observed in other ultralong waves. The variations of the baroclinic waves (m = 7-10) are more intermittent with a period of 4-5 days (not shown). This analysis indicates the importance of examining temporal variations of the energetics.

To examine the latitudinal variation of the energetics, monthly averaged values of M,L,F and D for each wavenumber are plotted against latitudes. The results for the zonal and for the first few wavenumbers are shown in Fig. 24.

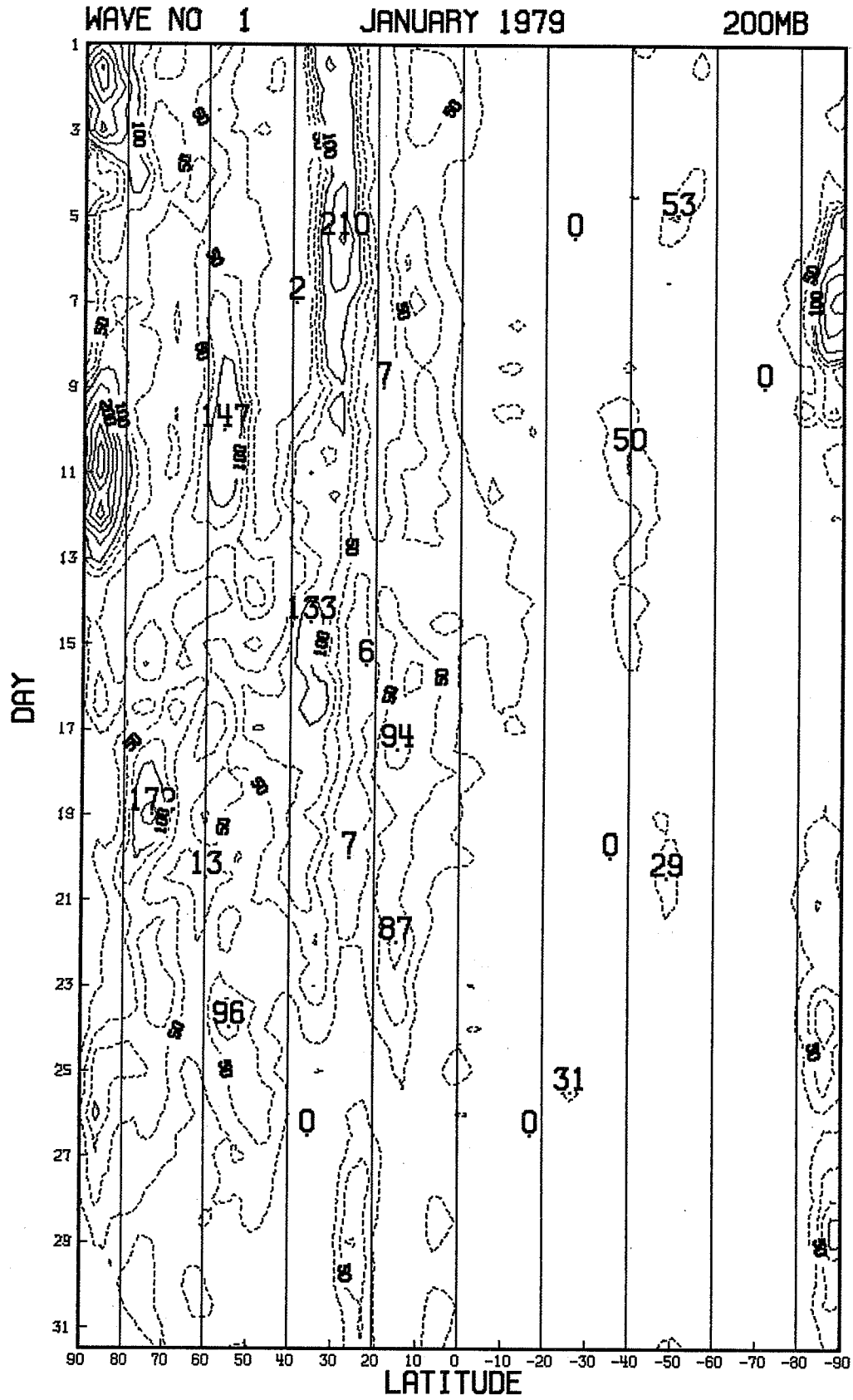

Fig.23 Latitude (abscissa) and time (ordinate) variations of the kinetic energy of zonal wavenumber 1. Unit in m^2 sec^{-2}. Contour interval, 25 m^2 sec^{-2}.

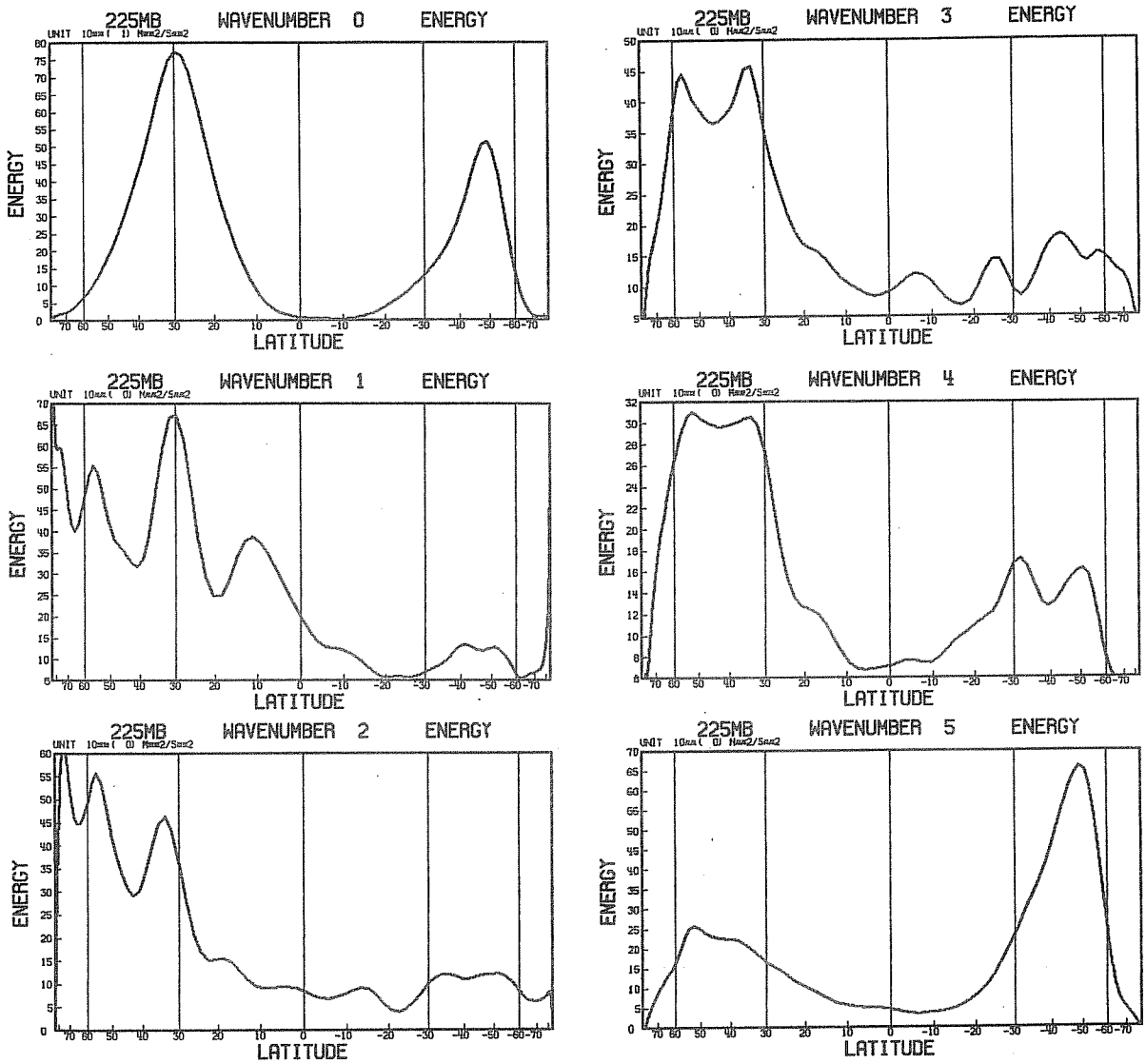

Fig.24a Latitudinal variations of the energy for various wavenumbers.
Note that the ordinate scales are not the same for all the waves.
The latitude scales are weighted by the area.

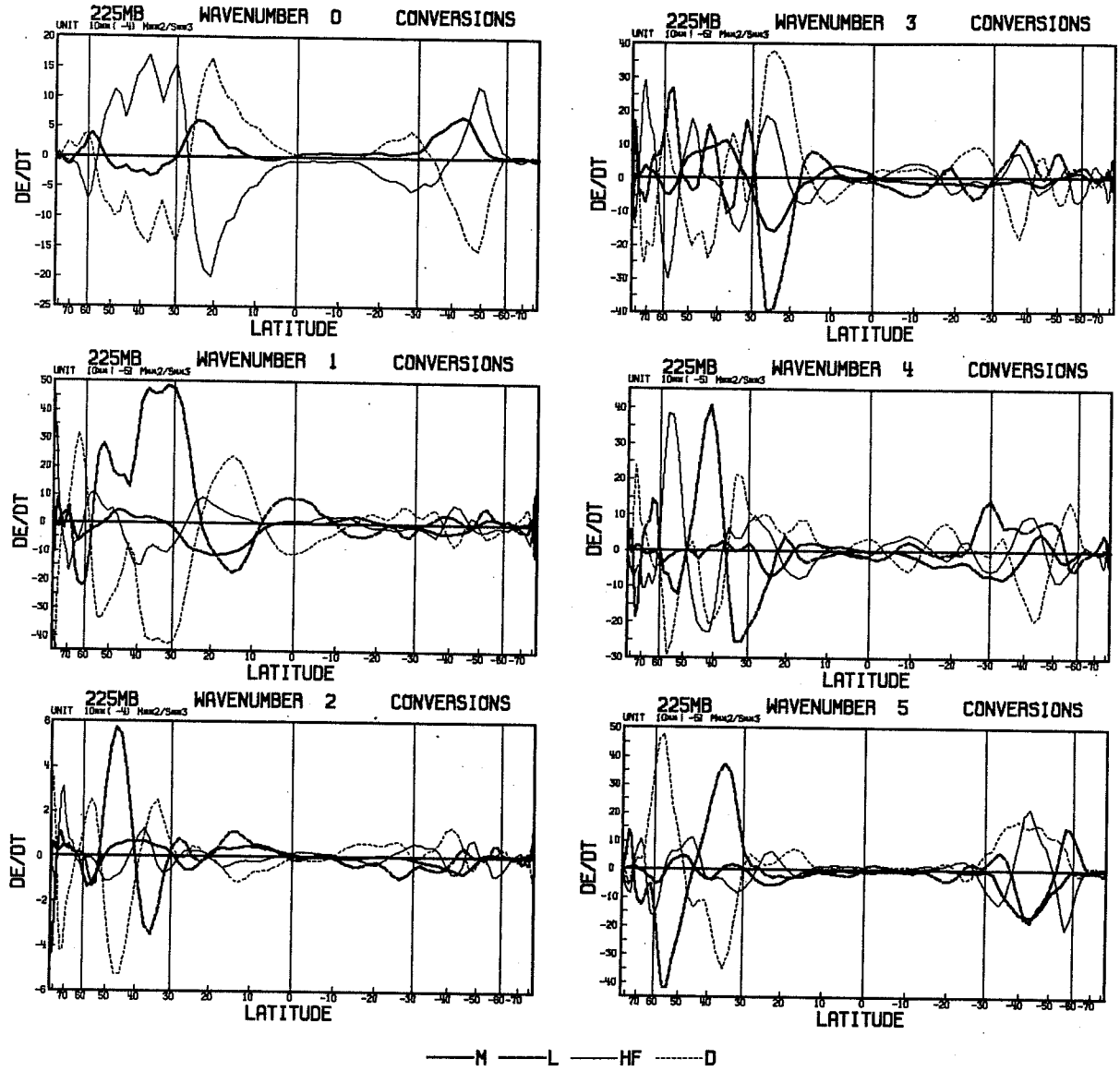

Fig.24b Same as Fig. 24a but for the energy conversions. Thick solid, thick dashed, thin solid and thin dashed lines indicate zonal-wave, wave-wave, flux and residual terms, respectively.

The zonal conversion (upper left figure) shows that the largest contribution to the zonal motion is the flux convergence term, negatively correlated with the smaller barotropic conversion term*. The distributions of these two terms indicate that the westerly momentum is generally transported northward in the northern hemisphere middle latitudes (southward in the southern hemisphere). The signs of M and F depend on the gradient of the zonal mean westerlies. The positive and the negative residual to the south and the north of the westerly jet indicates generation and destruction of the kinetic energy by the cross isobaric meridional circulation of the tropical Hadley and the middle latitude Ferrel cells, respectively.

The energetics of the waves show considerable variations with latitude. In general, magnitudes of the flux convergence terms are smaller than the scale interaction terms (L). By the careful examinations of Fig. 24, we are able to divide the northern hemisphere into three zones, which indicate quite different energetics among them.

4.4.1 Polar region (90^{o}N - 70^{o}N. Fig. 25, left)

The energetics in this zone is very much different from the other zones. The zonal motion provides large amount of energy to m = 1-6, indicating barotropically unstable nature of the waves. Energy exchanges between the waves show source of kinetic energy in m = 2 and 4, all other waves receiving energy from them. Since the actual wavelength for the given wavenumber is much smaller than that in the lower latitudes (about 14000 km for m = 1 at 70^{o}N), it may not be proper to use the word 'ultralong waves' in this zone. It is also difficult to classify baroclinic waves from this point of view. The relation with the evolutions of the stratospheric polar vortex seems to be essential in this region, but this is beyond the scope

---

* It may be misleading to call the term 'barotropic conversion', because the part of the flux convergence term contains wave-zonal interaction at the boundaries as shown in Appendix. The term M is more properly named as the transport of the westerly momentum up or down the gradient of the zonal westerlies. Similar terminology applies to L and F.

ENERGY DIAGRAM (NORTHERN HEMISPHERE) JANUARY 1979 250 mb–200 mb

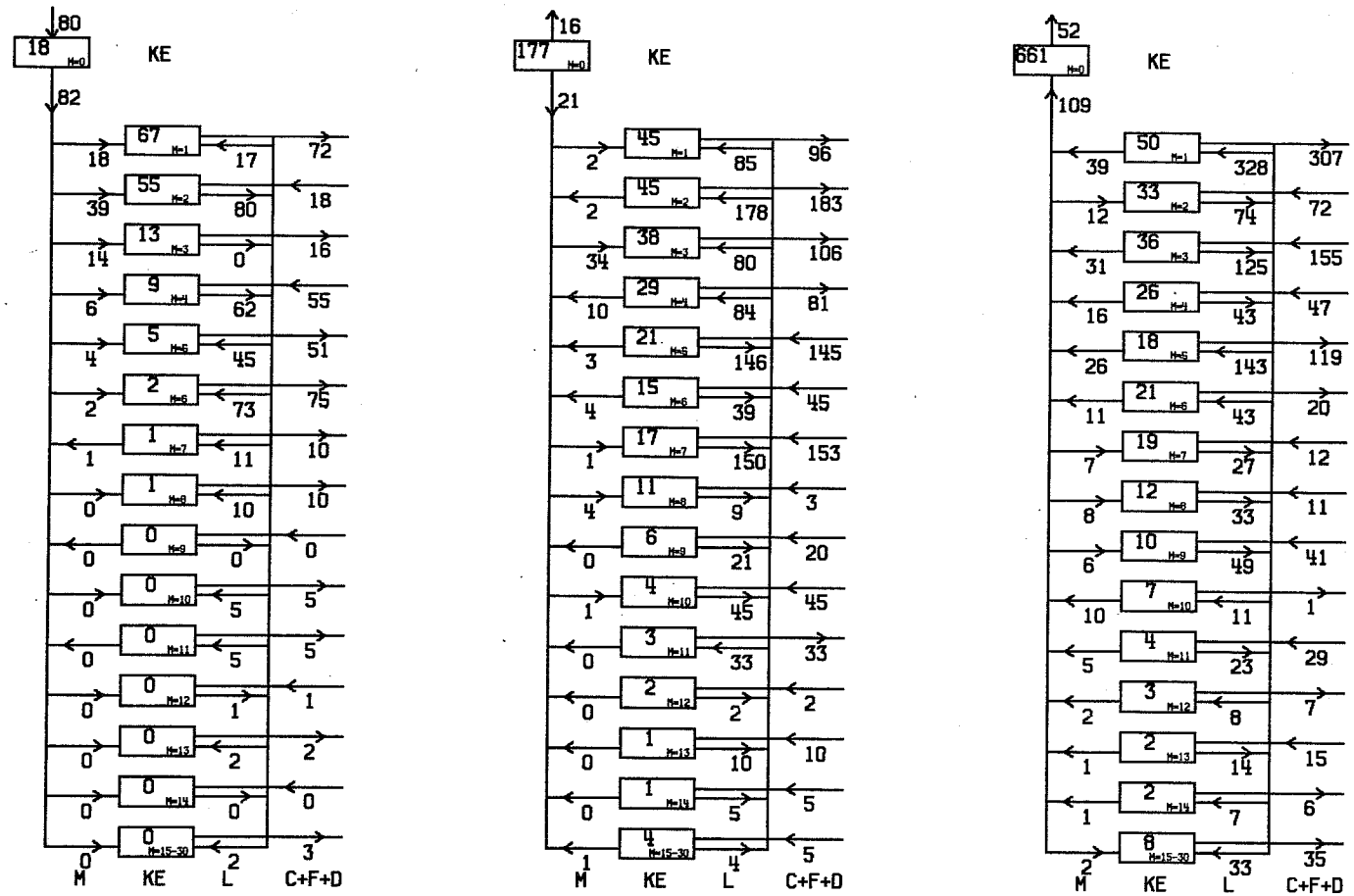

Fig.25 Same as Fig.22 but for the high latitude zones (left) middle latitude zones (centre) and for substropical zones (left)

of this study. The use of the zonal Fourier analysis may not be a proper method to decompose the scales in these high latitudes. The use of the spherical harmonics may be more appropriate.

4.4.2 Middle latitude zone (70°N - 40°N, Fig. 25, centre)

In this region, the zonal motion still provides its energy to the waves, mainly to m = 3. The role of wavenumber 3 as a drain on the energy of the zonal motion is noted by Wiin-Nielsen et al (1963) and Yang (1967). Conversions from all other waves are not significant (except m = 4 providing energy to the zonal). On the other hand, the wave-wave exchanges are significant. The kinetic energy sources exist in the baroclinic waves (m = 5-10), providing their energy to the ultralong waves (m = 1-4). Down the scale cascade of the energy is small. The residual terms of the ultralong waves are consistently negative. These energy exchange processes strongly indicate that the ultralong waves are dynamically forced (contrasted with thermally-forced) in these latitudes.

4.4.3 Subtropical zone (40°N - 20°N. Fig. 25, right)

This is the zone where the subtropical jet has its maximum intensity (30°N). The zonal to wave interaction reverses its sign from those in the other two areas, the zonal motion being maintained by the supply of kinetic energy from the waves. The wave-wave interactions are quite different from those in the middle latitude zone. The kinetic energy source exists in two scales, i.e. the baroclinic waves (m = 7-11, except 10), and the ultralong waves (m = 2-4) except wavenumber 1. A large amount of energy is transferred to wavenumber 1, which is consumed by the zonal-wave interaction, conversion to potential energy, flux across the boundaries, dissipation, etc. These conversions indicate that the forcings in the scale of m = 2-4, possibly by the heating and by the boundaries are essential in this area. It is noted that the major part of the Himalayas and some part of the Rockies are included in this zone, which may be related to the forcing in these scales. The strong sink of kinetic energy in wavenumber 1 is quite interesting. It indicates that this wave is dynamically forced through the interactions between the waves m = 2,3 and 4. The standing wavenumber 1 at 30°N corresponds to the strong jet centered around 150°E (see Fig. 9). The velocity potential pattern (Fig. 18, upper) suggests that there is a conversion from the potential energy to the kinetic energy around this longitude in the monthly averaged field. In

order to examine the differences of energetics between the standing part and the total part, complete energetics (including divergence related terms) are computed for the stationary part of the motion field (based on monthly averaged field), and shown in Fig. 26. It is noted that the vertical motion field over the high topography area may have significant errors. Generation of kinetic energy by the conversion from potential energy is clear in the area between 25^{o}N to 10^{o}N, supporting the qualitative estimates from the velocity potential field. The most significant difference with the total part (Fig. 24b, second from top left) is the magnitude of the wave-wave interaction terms (thick dashed lines), which indicate the dominance of the role of the transient wavenumber 1, the large temporal variations of the ultralong waves being noted in the beginning of this section (Fig. 23).

We have shown in this section that the latitudinal and temporal variations of the energetics of the ultralong waves are significantly large. This implies that the disagreement with other studies in the energetics in some of the wavenumbers should not be taken too seriously. Rather, it is more important to recognize the physical consistencies of the energetics obtained in this study.

5. SUMMARY AND CONCLUSIONS

The January 1979 analyses by the 4-dimensional assimilation scheme at the ECMWF using complete FGGE observations (II-b data sets) have been examined from climatological and kinetic energy budget studies.

The comparisons with the long time averaged January (and seasonal) climatologies indicate the following.

i) The northern hemisphere is somewhat anomalous due to the strong blockings persisting during the month.

ii) Significant differences in the flow fields over the oceans indicate the impact of the FGGE observations. The time variabilities of the motion field over the tropics in the upper troposphere are somewhat smaller than the climatological means. The momentum transports by the transient eddies are much smaller over the similar area and levels.

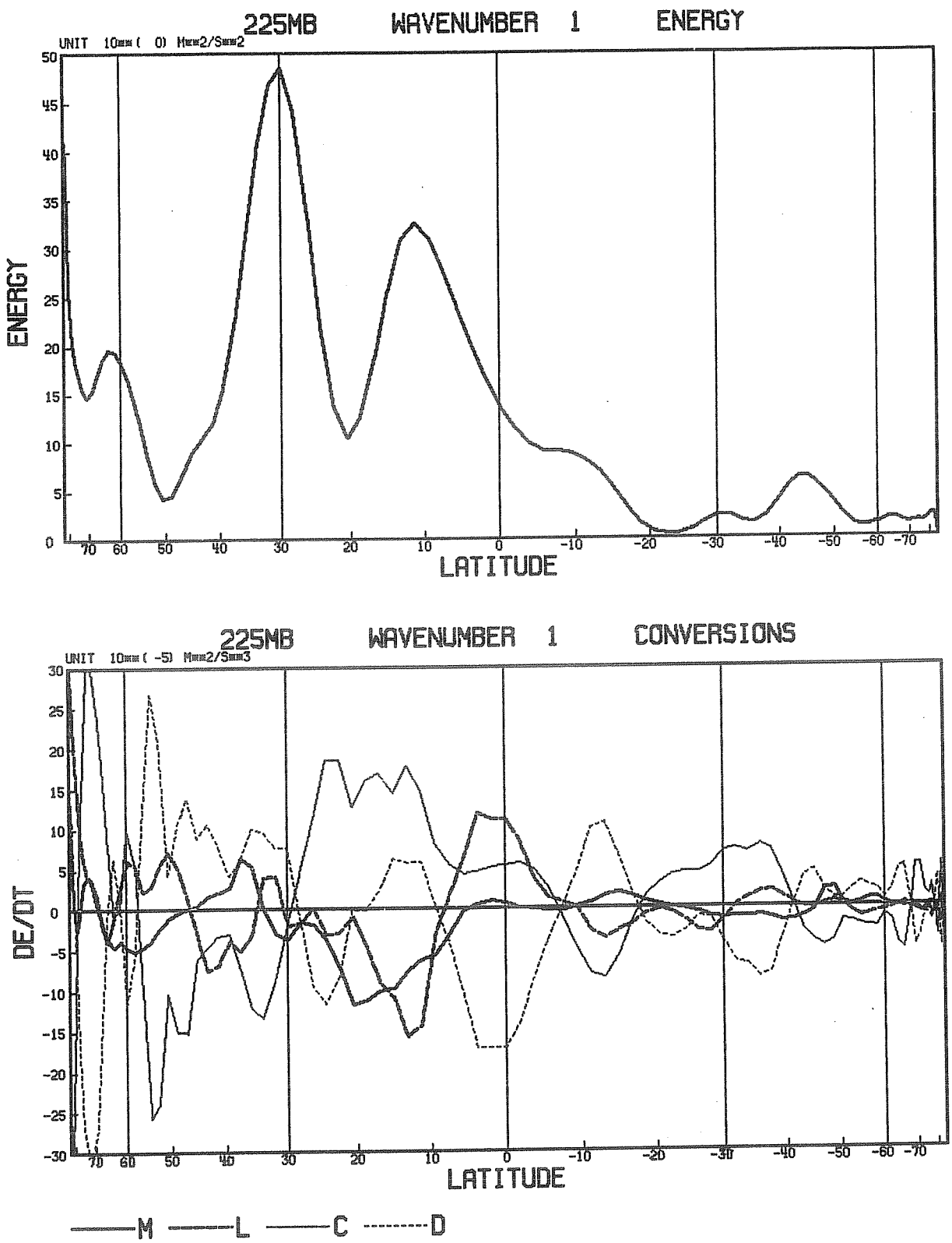

Fig.26 Latitudinal variation of the energetics of the stationary zonal wavenumber 1. Divergence related terms are included. Top panel is for the kinetic energy, bottom for the exchanges. Thick solid, thick dashed, thin solid and thin dashed lines indicate zonal-wave conversion, wave-wave conversion, baroclinic conversion and residuals, respectively. Note that the residual term implies dissipation as well as the contribution from the transient disturbances.

iii) In the southern hemisphere, surface highs and lows are more intense. Upper level flow patterns have more intense troughs and ridges, again indicating the impact of the FGGE observations. Momentum transports by the standing eddies are larger and the pattern different.

Since year to year variations can be significant, the above comparisons may not be entirely interpreted as the difference due to the observations coverage and the analysis scheme.

The analyses of the tropical divergence fields have been examined by mapping the velocity potential field. From the comparison with the initial guess field, a large part of the analyzed divergence has been found to be produced by the observations. The initialization procedure (nonlinear normal mode initialization) has a weakness of reducing the analyzed divergence in the tropics due to the lack of diabatic forcing.

The large scale velocity potential fields depict three local Hadley circulations between the areas of active tropical convection and the northern hemisphere continents, and the east-west circulations between the continents and the oceans in the southern hemisphere. The circulations have largest kinetic energy in the planetary boundary layer and at the tropopause.

A kinetic energy budget in the zonal wavenumber domain is performed on the analyses. The vertical motion field directly computed from uninitialized winds causes undesirably large residuals in computing the energy conversion terms. Other means of computing vertical motion must be investigated. The current computation excludes all the divergence related terms and includes them in the residual term.

The kinetic energy budget in the northern hemisphere agrees very well with the results compiled by Saltzman (1970), showing the role of baroclinic waves as kinetic energy sources for other scales of motion. The wave-wave interactions are stronger than the zonal-wave interactions also in agreement with Saltzman. Some differences are observed in the exchanges of each individual waves. In the southern hemisphere, the wave-zonal interaction dominates the wave-

wave interactions indicating the less important role of the ultralong waves and making clear contrast with the northern hemisphere energetics. The energetics in the tropics is quite different from those in high latitudes. The kinetic energy source is in the very large scale and the medium scale disturbances are maintained by receiving energy from very large scales. This result is similar to the energetics in the tropics during the northern hemisphere summer. Some discrepancies with the similar study by Krishnamurti et al (1974) during the northern hemisphere winter are found in the zonal-wave interactions of the ultralong waves, suggesting the sensitivities of the results to the analyses.

To examine further the energetics of the ultralong waves, latitudinal variations have been examined. The latitude-time variation of the kinetic energy of the ultralong waves shows narrow north-south scale (about 10° latitude from minimum to minimum) with large temporal variations. As a result, energetics of the ultralong waves changes significantly with latitude and time. The northern hemisphere is shown to be divided into several zones according to the different monthly averaged energetical nature of the motion field. Remarkable differences of the properties of the ultralong waves are found between the middle latitude zone (70°N - 40°N) and the subtropical zone (40°N - 20°N). In the middle latitude zone, all the ultralong waves are maintained by the baroclinic waves through the nonlinear interactions, while in the subtropical zone, ultralong waves except wavenumber 1 are also the energy sources for other waves. These energetics suggest that in the latter zone where nearly the entire Himalayas and part of the Rockies are included, the ultralong waves are externally (most likely thermally) forced and in the former zone they are dynamically forced by the interactions with the baroclinic waves. The wavenumber 1 in the subtropical zone has considerable time variability and the transient part are largely controlled by the nonlinear interactions among the waves.

The various climatological and energetics computations performed in this paper clearly reveals that the analyses of the FGGE data by the ECMWF 4-dimensional assimilation scheme are of good quality and suitable for diagnostic studies. The quantitative evaluation of the vertical motion field, however, still seems to have some difficulties. Use of the initialized field or other means have to be investigated depending on the purpose.

Applications of the analyses for relatively short time scale events (namely case studies) are not reported here. Preliminary study of the stratospheric sudden warming performed recently seems to indicate that the analyses are also physically consistent and useful in this respect.

Acknowledgements

The author gratefully acknowledges his colleagues of the FGGE group at the ECMWF for their help in performing this study. Dr. A. Simmons has been very helpful in improving the manuscript. Thanks are also due to Drs. L. Bengtsson, A. Hollingsworth and P. Julian for their many helpful discussions and comments.

APPENDIX

The conversion terms of the kinetic energy equation in the zonal wavenumber domain (Fig. 5) are expressed as follows.

(i) Zonal-wave interaction term (M)

$$M(m) = M_1(m) + M_2(m) + M_3(m)$$

$$M_1(m) = \frac{2}{a}\left\{\frac{\partial U(o)}{\partial \phi}\,\mathrm{Re}\,[U(m)\ V(-m)] + \frac{\partial V(o)}{\partial \phi}\,\mathrm{Re}\,[V(m)\ V(-m)]\right\}$$

$$M_2(m) = \frac{2\tan\phi}{a}\left\{U(o)\mathrm{Re}[U(m)\ V(-m)] - V(o)\mathrm{Re}[U(m)\ U(-m)]\right\}$$

$$M_3(m) = 2\left\{\frac{\partial U(o)}{\partial p}\,\mathrm{Re}\,[U(m)\ W(-m)] + \frac{\partial V(o)}{\partial p}\,\mathrm{Re}\,[V(m)\ W(-m)]\right\}$$

(ii) Wave-wave interaction term (L)

$$L(m) = L_1(m) + L_2(m) + L_3(m)$$

$$L_1(m) = -\sum_{k=1}^{\infty}\frac{2m}{a\cos\phi}\,\mathrm{Im}\,[\Psi(U,U,U) + \Psi(V,V,U)]$$

$$- \frac{2}{a}\,\mathrm{Re}\,[\Psi(\frac{\partial U}{\partial \phi},\ U,V) + \Psi(\frac{\partial V}{\partial \phi},\ V,V)]$$

$$L_2(m) = -\sum_{k=1}^{\infty}\frac{2\tan\phi}{a}\,\mathrm{Re}\,[-\Psi(U,V,U) + \Psi(V,U,U)]$$

$$L_3(m) = \sum_{k=1}^{\infty} 2\,\mathrm{Re}\,[\Psi(\frac{\partial U}{\partial p},U,W) + \Psi(\frac{\partial V}{\partial p},V,W)]$$

(iii) Baroclinic conversion term (C)

$$C(o) = -\frac{R}{p}\,W(o)''\ T(o)''$$

$$C(m) = -\frac{2R}{p}\,\mathrm{Re}\,[W(m)\ T(m)]$$

(iv) Flux term (F)

$$F(m) = F_1(m) + F_2(m)$$

$$F_1(o) = -\frac{1}{a\cos\phi}\frac{\partial}{\partial\phi}\cos\phi\left\{V(o)K(o) + 2U(o)\sum_{k=1}^{\infty}\mathrm{Re}\,[U(k)\,V(-k)] + 2V(o)\sum_{k=1}^{\infty}\mathrm{Re}\,[V(k)\,V(-k)]\right\}$$

$$F_2(o) = -\frac{\partial}{\partial p}\left\{W(o)K(o) + 2U(o)\sum_{k=1}^{\infty}\mathrm{Re}\,[U(k)\,W(-k)] + 2V(o)\sum_{k=1}^{\infty}\mathrm{Re}\,[V(k)\,W(-k)]\right\}$$

$$F_1(m) = -\frac{1}{a\cos\phi}\frac{\partial}{\partial\phi}\,2\,\cos\phi\left\{\sum_{k=1}^{\infty}\mathrm{Re}\,[\Psi(U,U,V) + \Psi(V,V,V)]\right\}$$

$$F_2(m) = -\frac{\partial}{\partial p}\,2\sum_{k=1}^{\infty}\mathrm{Re}\,[\Psi(U,U,W) + \Psi(V,V,W)]$$

(v) Pressure work term (W)

$$W(m) = W_1(m) + W_2(m)$$

$$W_1(o) = -\frac{g}{a\cos\phi}\frac{\partial}{\partial\phi}\cos\phi\left\{V(o)\,Z(o)''\right\}$$

$$W_2(o) = -g\frac{\partial}{\partial p}\left\{W(o)\,Z(o)''\right\}$$

$$W_1(m) = \frac{2g}{a\cos\phi}\frac{\partial}{\partial\phi}\cos\phi\,\mathrm{Re}\,[V(m)\,Z(-m)]$$

$$W_2(m) = -2g\frac{\partial}{\partial p}\,\mathrm{Re}\,[W(m)\,Z(-m)]$$

(vi) Dissipation term (D)

$$D(o) = U(o)\,X(o) + V(o)\,Y(o)$$

$$D(m) = 2\,\mathrm{Re}\,[U(m)\,X(-m) + V(m)\,Y(-m)]$$

(vii) Kinetic energy (K)

$$K(o) = \frac{1}{2} \{U(o)^2 + V(o)^2\}$$

$$K(m) = |U(m)|^2 + |V(m)|^2$$

In the above expressions, Ψ is an operator denoting,

$$\Psi(A,B,C) = A(m) \{B(-k)\ C(-m+k) + B(k)\ C(-m-k)\}$$

Im and Re denote imaginary and real part respectively.
The meaning of the symbols used are as follows

U(m) : zonal Fourier component of u

V(m) : zonal Fourier component of v

W(m) : zonal Fourier component of ω

X(m) : zonal Fourier component of the east-west component of the frictional force per unit mass.

Y(m) : zonal Fourier component of the north-south component of the frictional force per unit mass

Z(m) : zonal Fourier component of geopotential height.

R : gas constant of dry air

g : acceleration of gravity

p : pressure

ω : dp/dt

The double prime denotes the deviation from a north-south average:

$$\frac{1}{(\sin\phi_1 - \sin\phi_2)} \int_{\phi_1}^{\phi_2} A \cos\phi \, d\phi$$

The values in the diagrams (Figs. 23 and 26) are obtained by applying the above averaging procedures.

The divergence related terms are M_3, L_3, C, F_2 and W, which are set to zero in most of the computations, except in the case of the stationary part of the motion field.

References

Baer, F., 1972 An alternative scale representation of atmospheric energy spectra. J.Atmos.Sci., 29, 649-664.

Bengtsson L., and P. Kållberg, 1980 Numerical simulation - Assessment of FGGE data with regard to their assimilation in a global data set. Proceedings of the International Conference on Preliminary FGGE data analysis and results. Bergen, Norway (in press).

Chen, T.C. and Wiin-Nielsen, A., 1976 On the kinetic energy of the divergent and nondivergent flow in the atmosphere. Tellus, 28, 486-497.

Krishnamurti, T.N., 1971 Tropical east-west circulations during the northern summer. J.Atmos.Sci., 28, 1342-1347.

Krishnamurti, T.N., M. Kanamitsu, W.J. Koss and J.D. Lee, 1973 Tropical east-west circulations during the northern winter. J.Atmos.Sci., 30, 780-787.

Lorenc, A., I. Rutherford and G. Larsen, 1977 The ECMWF analysis and data assimilation scheme - Analysis of mass and wind fields. ECMWF Tech. Report No. 6. Shinfield Park, Reading, England, 47 pp.

Lorenc, A.C. 1980 A global three-dimensional multivariate statistical interpolation scheme. Proceedings of the International Conference on Preliminary FGGE Data Analysis and Results. Bergen, Norway (in press).

Newell, R.E., J.W. Kidson, D.G. Vincent and G.J. Boer, 1972 The General Circulation of the Tropical Atmosphere and Interactions with Extratropical Latitudes. Vol. 1. The MIT Press, Cambridge, Mass., USA and London, UK, 258 pp.

Oort, B., 1957 On estimates of the atmospheric energy cycle. Mon.Wea.Rev., 92, 483-443.

Saltzman, B., 1957 Equations governing the energetics of the large scales of atmospheric turbulence in the domain of wave number. J.Meteor., 14, 425-431.

Saltzman, B., 1970 Large-scale atmospheric energetics in the wavenumber domain. Rev.Geophys., 8, 289-302.

Wiin-Nielsen, A., J.A. Brown and M. Drake, 1963 On atmospheric energy conversions between the zonal flow and the eddies. Tellus, 15, 168

Yang, C.H. 1967 Nonlinear aspects of the large scale motion in the atmosphere. Sci. Rept. No. 08759-1-T, Dept. of Meteorology and Oceanography, University of Michigan, Ann Arbor.